Summer 8-3-2018

A Study of Exposure to Polycyclic Aromatic Hydrocarbons and Polymorphisms in the Tumor Suppressor Gene, p53, of Wild Menhaden

Samantha Rose Reed
samantha.reed@student.shu.edu

A Study of Exposure to Polycyclic Aromatic Hydrocarbons and Polymorphisms in the Tumor Suppressor Gene, p53, of Wild Menhaden

Samantha Rose Reed

Submitted in partial fulfillment of the requirements for the degree of Master of Science in Biology from the Department of Biological Sciences of Seton Hall University

August 3, 2018

Approved by

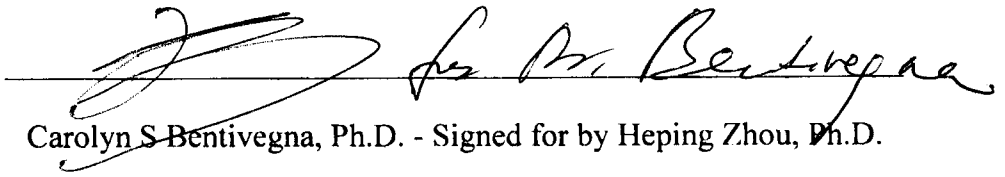

Carolyn S Bentivegna, Ph.D. - Signed for by Heping Zhou, Ph.D.

MENTOR/ COMMITTEE MEMBER

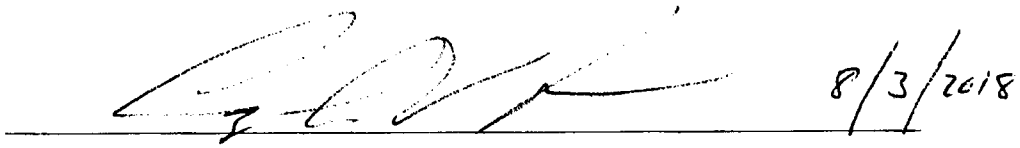

Angela Klaus, Ph.D.

COMMITTEE MEMBER

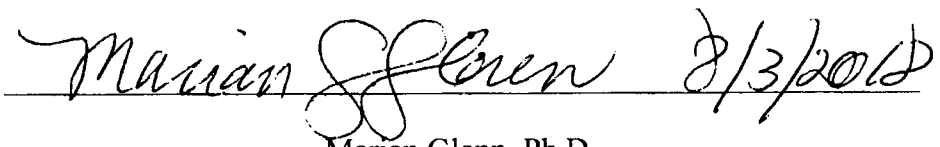

Marian Glenn, Ph.D.

COMMITTEE MEMBER

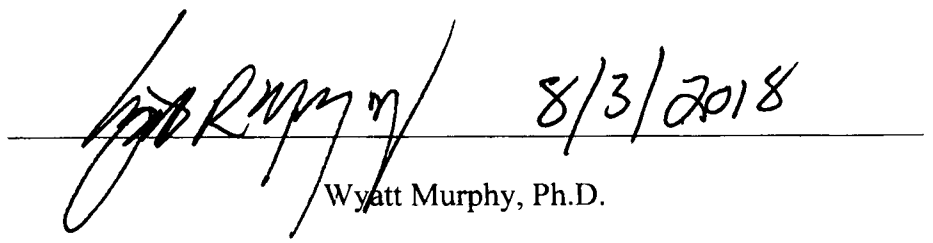

Wyatt Murphy, Ph.D.

COMMITTEE MEMBER

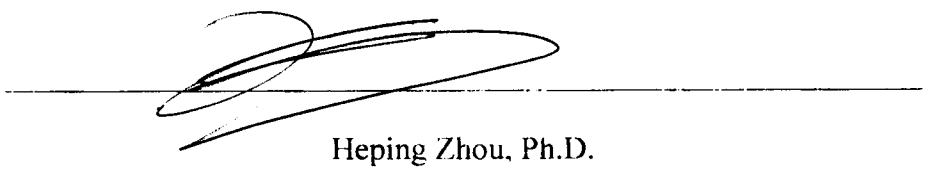

Heping Zhou, Ph.D.

CHAIRPERSON, BIOLOGY DEPARTMENT

Acknowledgements

The path towards this master's thesis has been unconventional. Its completion is thanks in large part to the special people who challenged, supported, and stuck with me along the way.

I am highly indebted to the faculty and professors at Seton Hall University for their guidance and constant support for both my undergraduate and graduate degrees furthermore allowing me to fulfill this endeavor.

I am tremendously fortunate to have committee members Dr. Wyatt Murphy, Dr. Marian Glenn, and Dr. Angela Klaus. I thank them for supporting this project and giving such thoughtful feedback, always aimed at moving me forward.

It is a genuine pleasure to express my deepest sense of gratitude and appreciation to my mentor, Dr. Carolyn S. Bentivegna. Without her enthusiasm, support, encouragement, and above all continuous dedication to this work this study would have hardly been completed. Your kindness, expert advice, meticulous scrutiny, and scholarly knowledge is deeply missed.

Finally, and most importantly, I owe a great debt of gratitude to my family and close friends for their constant encouragement, patience and understanding.

Table of Contents **Page number**

Abstract

The British Petroleum (BP) Deep Water Horizon Oil spill in the Gulf of Mexico (GOM) caused detrimental effects to wildlife including marine fish populations (Diercks, et al. 2010). The fish were exposed to crude oil which contains polycyclic aromatic hydrocarbons (PAHs). Some PAHs are carcinogens and can damage DNA in key regulatory genes in various species (Milleman, et al. 2015; Nadler, 2017). Menhaden are oily, filter feeding fish and incorporate and retain these lipophilic contaminants at high levels. The objective of the present work was to search for genetic mutations on the tumor suppressor gene, *p53*, in various organs (gill, muscle, gonad, liver, and heart) of wild menhaden collected from two locations with differing proximity to the spill. Gulf Menhaden (*Brevoortia patronus*) were collected from the Vermillion (low oil exposure) and Grand Isle (heavy oil exposure) bay areas of the GOM. The DNA binding region of the *p53* gene was amplified by PCR and Single-strand Conformational Polymorphism (SSCP) was utilized as an indicator of *p53* mutations. *P53* normally functions to inhibit cell division when excessive DNA damage is present. When mutated, cancer may result from uncontrolled cell growth. Fluorescence spectroscopy confirmed PAH- like compounds in almost all fish samples tested. The genomic analysis illustrates one sharp band at 360 bp which is consistent with the expected size of the DNA binding domain of *p53*, indicating a successful amplification of this gene. SSCP reveals one profile in all organ samples concluding low incidence of gene variation or single nucleotide polymorphisms.

Introduction

A natural experiment began in 2010 when the British Petroleum drilling rig in the Mississippi Canyon exploded releasing over 210 million gallons of crude oil in the Gulf of Mexico across 1300 miles of shoreline (McCann et al., 2017). This explosion killed 11 workers and leaked crude oil for 87 days, releasing approximately 800 thousand gallons per day before being capped (McCann et al., 2017).This spill caused detrimental effects to a plethora of fisheries and wildlife. Fish were exposed to highly toxic crude oil. Abundant among the various constituents of crude oil, is a class of hydrocarbons known as polycyclic aromatic hydrocarbons (PAHs) known to have potent mutagenicity and to play a critical role in the causation of cancer (Ozhan, et al. 2014).

Crude oil is composed of a variety of hydrocarbons distinguished as paraffinic, naphthenic, and aromatic (Shukla, 2012). Paraffinic hydrocarbons are saturated and known as alkanes; either straight-chained or branched. These hydrocarbons are the major constituents of natural gas and petroleum which normally contain 5-15 carbon atoms per molecule (Harvey, 1997). Naphthenic hydrocarbons are utilized for all liquid refinery products where the hydrocarbon structures are ringed with one or more rings containing only single bonds. The third and final category is aromatic hydrocarbons or polyarenes which are common building blocks in the petrochemical industry where the hydrocarbons form aromatic structures with one or more benzene rings fused together (Singleton et al., 2016). For this present study, polycyclic aromatic hydrocarbons were evaluated because they are the major chemical constituent in crude oil.

Polycyclic aromatic hydrocarbons (PAHs) are a versatile class of organic molecules composed of two or more covalently bound aromatic rings and are nonpolar, chemically-stable

molecules with low volatility and aqueous solubility. Their versatility is primarily due to the catenation or “self-bonding” of carbon molecules which prevents saturation of the hydrocarbons to produce kinks, which allows PAHs to be sequestered in bay or estuary sediments for prolonged periods of time to cause further harm (Bentivegna, 2016). Major sources of (PAHs) in the environment are due to crude oil spillage (petrogenic sources) and from the incomplete combustion of fossil fuels and other organic matter mainly by burning coal, oil, gasoline, tobacco, wood, and other organic substances contributing to over 50% of nationwide emissions (pyrogenic sources) (Retzlaff et al., 2013). Other sources of exposure include vehicle exhaust emission, eating contaminated food sources, air pollution, and drinking contaminated water which contributes 35% of exposure (Sunnucks et al., 2000).

These carcinogenic contaminants are also formed through pyrolysis of terpenes through burning renewable energy resources such as wood and agricultural waste. (Rust et al., 2004). In this case an alternative energy source used for environmental benefit creates precursors to environmental pollutants. The process is initiated when PAHs arise through pyrolysis when free radicals undergo a series of reactions to form larger ring structures or high molecular weight PAHs strongly associated with carcinogenicity. The Diels-Adler slow condensation reaction of butadiene, in particular, is thought to play a critical role in the mechanistic pathways involving free radicals. This reaction entails an electron-rich compound such as a diene attacking an electron deficient compound, a dienophile (Llamas, et al. 2017). In addition, the substitution of polyarenes strongly influences their carcinogenic properties: two or more methyl substitutions giving enhanced activity while a methyl substitution in the benzo ring diminishes activity (Song, 2009). The position of the alkyl substituent is also critical in determining carcinogenicity. Harvey (1997) reported that the 7- and 12-ethyl positions on a polyarene are strongly

tumorigenic due to their intercalation of PAHs between base pairs of the DNA helix. Through substitution, methylation, and alkylation both electron donating and electron accepting groups can enhance susceptibility to cancer.

According to the quantum mechanical theories of carcinogenicity, there are three distinct structural regions that strongly influence the potent carcinogenic nature of these molecules. The first is the *k-region* formed by the angular fusion of two aromatic rings which is viewed as a carbon-carbon double bond (Harvey, 1997). The second is the *L-region* which appears in a meso molecular region viewed as single carbon bond. The final region is the *m–region* which appears as a ring with 4 carbon exposed bonds to play a critical role in the metabolism of these molecules (Harvey, 1997**). Figure 1** conveys the regions of the KLM theory which is a predicative indicator on carcinogenicity. Carcinogenic polyarenes possess all three of these structural regions, in addition to having methyl groups at molecular sites which enhance oncogenic activity (Harvey, 1997).

Previous studies indicate a strong correlation between exposure to polycyclic aromatic hydrocarbons and the etiology of certain cancers (Goto,2011). Exposure to benzo[a] pyrene, a prevalent PAH, is associated with an increased incidence of skin and lung cancer. Goto (2012) reports that, the PAH exposure was monitored and validated through PAH metabolites excreted in the urine, DNA adducts, and immunohistochemistry staining on tissues. The strong correlation between tumorigenicity and chemical properties of polyarenes supports the significance of measuring genotoxicity in aquatic organisms for biomonitoring effects of aquatic crude oil spills.

Since crude oil consists of low and high molecular weight PAHs, the light compounds are subjected to natural weathering processes (evaporation, biodegradation, photo-oxidation).

High molecular weight PAHs persist in the ocean for extended periods of time easily accessible for marine life. The fish of interest are menhaden (Family *Clupeidae*, Genus *Brevoortia*) which are exceedingly oily consequently giving them a higher chance to incorporate and retain these lipophilic contaminants. As menhaden are ubiquitous prey fish, predatory fish such as: silver perch, bluefish, white bass, tuna, mackerel, and salmon can readily absorb and bioamplify the PAH contamination, thereby affecting marine ecosystems (Bentivegna, 2016). There are four species of menhaden that live in the coastal waters of North America: *Brevoortia tyrannus, B. smithi, B. patronus, and B. gunteri* (Pena, 2015). In addition to their oily nature, their risk of exposure is enhanced by a unique filter feeding lifestyle by incorporating materials through their open mouths while filtering out the undesirable parts through their gills. These migratory fish are an essential and critical part of maintaining the aquatic environment via serving as part of the food chain that is a major link between producers and secondary consumers in key locations within estuaries and coastlines. Many of these fish, such as Atlantic menhaden, located on the East Coast spanning down to the Gulf of Mexico, are not directly used for food but are eaten by many commercially important fish as well as used for livestock feed and processed into fish oil and fish meal that is used for dietary supplements (Milleman et al., 2015). However, these high-demand species are greatly susceptible to large-scale anthropogenic pollution caused by major oil spills, such as the 2010 British Petroleum Deepwater Horizon Oil spill, where contaminants, such as polycyclic aromatic hydrocarbons directly harm species like Menhaden through genotoxicity.

Since PAHs are highly lipid soluble, they are absorbed readily through the gastrointestinal tract and distributed throughout various organs with an increased localization and retention in the adipose tissue until further metabolism and/or excretion occurs. Chemical

carcinogens such as PAHs are known to be metabolized in the microsomes on the endoplasmic reticulum which increases their toxicity. The metabolism of PAHs occurs through activation facilitated by two groups of enzyme systems known as Phase 1 and Phase 2. An essential Phase 1 enzyme is cytochrome P-450, which is critical in producing the carcinogenic metabolites (Harvey, 1997). Some PAHs are known to be long-lasting carcinogens that damage DNA, in particular key regulatory genes such as proto-oncogenes or tumor suppressor genes in various species (Mordukhovich, et al. 2010). For this reason, there is a great environmental concern regarding PAH mutagenesis of critical regulatory genes like tumor suppressor gene, *p53,* which is essential for inhibiting cell growth and inducing apoptosis (Mordukhovich, et al., 2010).

The tumor suppressor gene *p53,* commonly known as "the guardian of the genome" is essential in suppressing cancer by conserving stability to prevent genomic mutations from spreading (Schaefer et al.,2015). The structure of *p53* consists of the amino terminus (transactivation) domain, proline-rich domain, DNA binding domain, and oligomerization domain (Saha, 2015). Each domain functions respectively, to activate downstream target genes, mediate *p53* responses to DNA damage to initiate apoptosis, activate transcription factors, and interact with monomers to mediate dimerization (Nomura et al., 2011). When defective, uncontrolled cell growth is exhibited which is a hallmark of various cancers. Polymorphisms in the Menhaden tumor suppressor gene may occur due to the genotoxicity of environmental PAHs. This would establish a link between PAH exposure and cancer in wild menhaden. The rationale for focusing the present study on *p53* is to identify a mutagenic effect from PAHs on a cancer-related gene. For this reason, *p53* polymorphisms were chosen as the model biomarker of environmental exposure to PAHs in aquatic species.

For this study, the objective was to explore the genetic effects of PAH contamination from a massive petrogenic event on aquatic species. Furthermore, this would allow the investigation of the presence of *p53* polymorphisms in a wild population of Gulf menhaden to further determine a relationship between the amounts of *p53* polymorphisms and PAH contamination in various organs. Gulf menhaden (*Brevoortia patronus*), were collected post-BP oil spill, and the presence and quantities of PAHs were determined using Excitation-Emission Matrix scans (EEMs). DNA was isolated from the gill, muscle, gonad, liver, and heart of individual fish, amplified by polymerase chain reaction (PCR) and analyzed through single-strand conformational polymorphism to detect polymorphisms associated with amplicons of various size. The end result was to determine the relationships between PAH-like compound concentrations in various organs and determine if certain organs were more susceptible to polymorphisms than others in respect to PAH damage.

Figure 1: K, L, M regions of an aromatic compound. Derived from ChemDraw (license by Seton Hall University libraries)

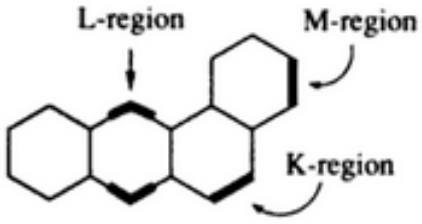

Materials and Methods

Fish Sample Collection Sites

Gulf menhaden (*Brevoortia patronus*) were caught by Louisiana Fish and Wildlife Service in the fall of 2012 and 2013 from two locations along the Gulf of Mexico more than 250 miles apart (**Fig. 2**). One site was in Barataria Bay, Louisiana, near Grand Isle (GILA) which directly received heavy oiling from the Deepwater Horizon (DWH) oil spill in 2010. The second site was in Vermillion Bay (VBLA), Louisiana, which received less impact from the oil spill and served as a reference site (Pena, 2014). The fish were collected by gill net and trawling, kept frozen and sent to Seton Hall University (South Orange, NJ). The fish were labeled and stored in a -20 °C freezer for further processing.

Figure 2: Map of Vermillion Bay (VBLA) and Grand Isle bay (GILA), two sampling sites for Gulf menhaden (*Brevoortia patronus*) in the Gulf of Mexico.

http://jerrylabella.com/louisiana-fishing-maps

PAH Extraction

The fish were dissected upon thawing on ice. Fish organs (heart, liver, muscle, gill and gonad) were excised and stored frozen at -20 °C. A 0.05 g sample of intact liver, heart, muscle, gill, and gonad from each fish was homogenized in 1 mL 75% ethanol (75% ethanol/water v/v). A 100 µL of each organ homogenate was added to 900 µL of 75% ethanol. The mixture was vortexed for 1 min and then centrifuged for 20 min at 13,000 rpm at 4 °C (Prism R™ Refrigerated MicroCentrifuge). The supernatant, containing the PAH extraction, was removed for fluorescence analysis. All ethanol in this study was KOPTEC 200 proof (VWR International, King of Prussia, PA, USA). Dilutions were made with 18 ohm water from a Milli-Q-Integral 5 (EDM Millipore Inc., Billerica, MA, USA).

PAH Standards and Other Aromatic Standards

PAH and suspected metabolite standards were obtained from Sigma-Aldrich. They were 2-naphthol, 9- phenanthrol, 1-hydroxypyrene, benzo[a]pyrene, and benzo[b]fluoranthene. Other standard compounds from Sigma-Aldrich were bovine serum albumin, NADH, vitamin E, and vitamin A. The PAH standards, vitamins and albumin were dissolved in 75 % ethanol for fluorescent analysis. The structures of the PAH standards were derived from ChemDraw (license by Seton Hall University libraries). PAH standards were scanned previously with Fluorolog®3 in the lab by previous graduate students (Pena, Ridley, 2014).

Fluorescent Analysis of PAHs in Fish Samples

Fish liver, gonad, gill, heart and muscle sample supernatants, containing PAHs, were subjected to fluorescent analysis on a Fluorolog® 3(Horiba Jobin Yvon, Inc., Edison, NJ, USA) with 1 cm excitation light path length. The supernatants were transferred in semi-micro 1 mL fused silica cuvettes (Starna), and analyzed by scanning the excitation wavelength between 260-400 nm and recording the emission wavelength between 320-480 nm. The wavelengths were adapted from PAH standards that were scanned previously with Fluorolog®3 in the lab (Pena, Ridley, 2014). In addition, raw crude oil from the spill was extracted into 75 % ethanol to serve as a positive control. The procedure for analysis was the same as viewing the various organ homogenates. The intensity of the emission signal is displayed as a false color map in units of cps/mV.

3D contour maps, showing excitation scans for multiple emission wavelengths and fluorescence intensity were generated in SigmaPlot 14 (license by Seton Hall University libraries) from the EEMs data. The contour maps display 3D data as heat maps with the red color representing highest intensity and blue color representing lowest intensity fluorescence. The contour map also differentiates fluorescence compounds based on their optimal emission and excitation wavelengths (Nadler, 2017).

DNA Extraction from the Fish Samples

Genomic DNA was extracted using DNAzol (Thermo-Fisher, cat# 10503027) following the supplier's protocol with some modifications. A 0.05 g sample of fish muscle, gill, liver, or heart was homogenized in 1 mL DNAzol and centrifuged (10,000 rpm, °C, 10 min) to remove

cell solids. The supernatant was kept and 500 µL of 100% ethanol added to precipitate the DNA. The mixture was centrifuged, and the supernatant was removed. The pellet obtained was washed twice with 75% ethanol. After the final wash, the supernatant was removed, and the DNA pellet was air dried for approximately 1 min. The DNA was further purified by re-dissolving in 200 µL of 8 mM NaOH (Sigma Aldrich) and centrifuging at 12,000 rpm for 10 min at 4 °C. An aliquot of the supernatant containing purified DNA, was analyzed for DNA purity and concentration using a UV/Vis Spectrophotometer (DU 730 Life Science, Beckman Coulter Inc., Jersey City, NJ, USA) at 260 nm, 280 nm, and 320 nm. The remaining supernatant was transferred into a new microcentrifuge tube containing 12.04 µL of 0.1 M sterile pH 7.5 HEPES solution (AMRESCO, Solon, OH, USA) for storage at -20 °C.

PCR and Gel Electrophoresis of beta-actin to Validate DNA Isolation

To validate effectiveness and integrity of DNA isolation, two of the DNA samples, GILA 554 L and VBLA 271 L, were subjected to PCR using primers for the *Fundulus heteroclitus* beta-actin housekeeping gene. PCR samples were composed of 12.5 µL Gene Amp Fast PCR 2X Master Mix (Applied Biosystems, Warrington, MA, UK), 8.5 µL Molecular Grade Water (Mediatech, Inc., Manassas, VA, USA), 2 µL of appropriate DNA, 1 µL of appropriate forward primer, and 1 µL of appropriate reverse primer (Nadler, 2017) PCR reactions were run on a Gene Q Thermal Cycler (Model TC-24/H(b)) with parameters of 3 min at 95 °C, followed by 45 cycles of 1 min at 95 °C, 1 min at 60 °C, and 1 min at 72 °C, and ending with 72 °C for 3 min. Samples were then held at 4 °C in the machine until analysis by gel electrophoresis.

For gel electrophoresis, a 2% agarose gel was prepared. The gel was made by combining 0.9 g of UltraPure agarose and 45 mL of 0.5X trisborate EDTA (TBE) buffer diluted from

UltraPure 10X TBE stock (Life Technologies, Grand Island, NY, USA). This combination was then put in the microwave for 30 seconds and repeated until agarose was dissolved in the 0.5X TBE solution. A 2 µL amount of 10 mg/mL ethidium bromide (Invitrogen, Carlsbad, CA, USA) was pipetted into the agarose solution. After the gel solidified and cooled, the solution was poured into a small agarose tray. 6 µL of each sample was combined with 2 µL of 3X loading buffer (Invitrogen TrackIt Cyan/Yellow) and then loaded into the gel. The samples were run alongside an Invitrogen 100 bp DNA ladder with 2 µL of 0.5 µg/µL DNA marker ladder combined with 2 µL of loading buffer. 250 mL of 0.5X TBE buffer was poured into the gel apparatus tank. The gel was run for 1 hr at 72 V. The DNA bands were visualized by observing the intercalated ethidium bromide fluorescence through a UV transilluminator (Proteinsimple, Santa Clara, CA, USA).

p53 Primer Design and Verification

Amplification of the target DNA, i.e. *p53* DNA binding domain, was conducted with *p53* primers designed from an Atlantic killifish (*Fundulus heteroclitus*) transcriptome for *p53* due to the killifish transcriptome having high similarity to the Menhaden transcriptome (Zadlock). The *p53* DNA binding domain location oriented at 105-254 base pairs was verified using the European Molecular Biology Laboratory – The European Bioinformatics Institute (EMBL-EBI) pfam service (http://pfam.xfam.org/). The aligning of the NCBI FASTA nucleotide sequence and the amino acid sequence of the functional domain of the protein from *Fundulus heteroclitus* showed a (99%) amino acid sequence alignment match.

The forward primer selected (F4) started at base pair 8 and the reverse primer (R0) started at base pair 342 allowing for a 360 amplicon. The oligonucleotide sequences of the

primers were checked to ensure minimal self–dimerization, hairpin, and heterodimerization by running the sequences through Integrated DNA Technologies (IDT) OligoAnalyzer 3.1. (http://www.idtdna.com/calc/analyzer). Two other primers were designed but not used. **Table 1** and **Figure 3** below show the primer design and amplicon region.

Primer design	Start location	Oligonucleotide size (bp)	Sequence
Forward (4)	7	20	5'GACCACCATTCTTCTCAGCT3'
Reverse (0)	342	20	5'TTGCTGTCGCTTTTCTCCTT3'

Table 1: Primer design and amplicon region of forward and reverse primer set F4R0.

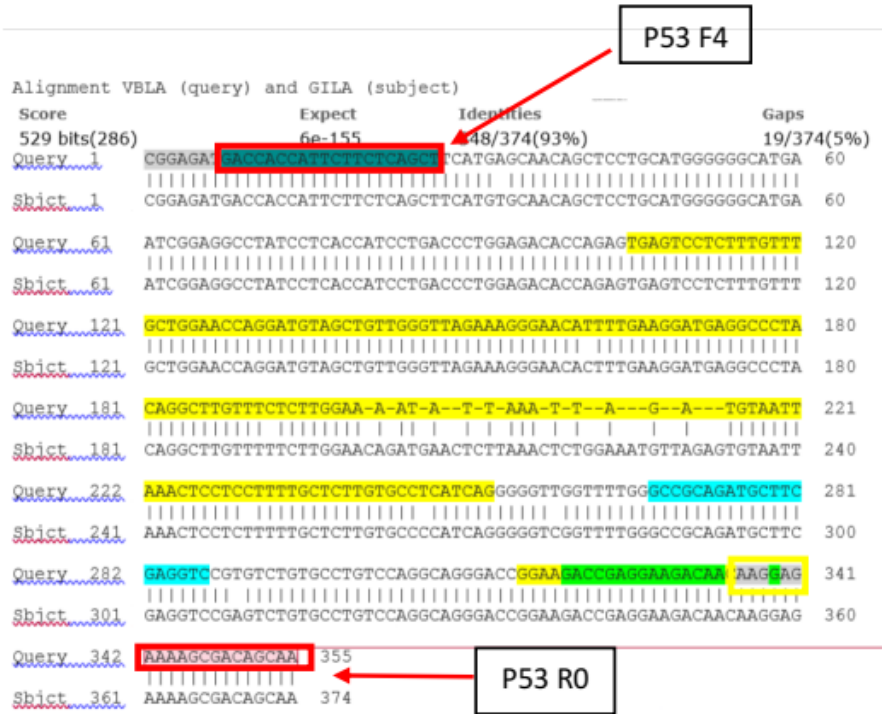

Figure 3: Alignment of primer design of intended amplicon region of primer set F4R0.

PCR and Gel Electrophoresis for p53 DNA Binding Domain

The target DNA, *p53* DNA binding domain, from the fish samples were amplified using PCR. PCR reactions and gel electrophoresis were set up as described previously using the *p53* DNA binding domain primer set. The PCR parameters were 2 min at 95 °C and 35 cycles of 1 min at 95 °C, 1 min at 60 °C, 1 min at 72 °C, ending with 72 °C hold for 7 min. All subsequent PCR reactions were run with these parameters. The amplified DNA was checked by agarose gel electrophoresis as previously described to ensure only a single DNA band of expected 360 bp size.

Cloning and Sequencing of the p53 DNA Binding Domain

The cloning procedure followed was that provided in the TOPO® TA CLONING Kit (ThermoFisher, cat# K457502). The cloning reaction was composed of 2.5 µL of PCR product, 1 µL of salt solution (1.2 mM NaCl, 10mM $MgCl_2$), 1.5 µL water, and 1 µL of TOPO® vector. The mixture was incubated on ice for 15 min, then a 2 µL aliquot was added to the One Shot® TOP 10F' chemically competent *E. coli* cells. This was gently mixed then heat shocked at 42 °C for 30 s then immediately chilled on ice. A 250 µL aliquot of room temperature super optimal broth with catabolite repression (SOC) media which is utilized to obtain maximal bacterial cell transformation was added to the cells, and then incubated while shaking at 37 °C for one hr. Cells were then spread onto pre-warmed 100 µg/mL LB-ampicillin plates that had been treated with 80 µL of 20 mg/mL X-Gal and 40 µL of 20 µg/mL IPTG (isopropyl β-D-1 thiogalactopyranoside) and incubated at 37 °C overnight. All subsequent cloning in this study followed this exact procedure (Thermo Fisher Scientific, Waltham, MA, USA).

The positive clones were sequenced after PCR amplification. To do this, three white colonies, indicating the successful insertion of target DNA in the bacterial plasmid, from each plate, were selected and suspended in 50 µL of Molecular Biology Grade Water (Thermo Fisher, Waltham, MA, USA) and was used as DNA template. A PCR was run using the *p53* forward primer and the plasmid specific M13 reverse primer from the cloning kit. The PCR products, after verification on successful agarose gel electrophoresis, were sent out for sequencing (GenScript DNA Sequencing Service, GenScript Biotech Corporation, Piscataway, NJ, USA) to validate the amplification of the *p53* DNA binding domain.

Single Strand Conformation Polymorphism (SSCP) Analysis of p53 DNA Binding Domain

The amplified *p53* DNA binding domains from all samples were analyzed for polymorphisms with the Single Stranded Conformational Polymorphism (SSCP) technique using vertical gel electrophoresis with Mini-PROTEAN® TBE Precast Gels (BIORAD, Cat# 165-8000). The gel was placed in the alignment slot of the casting stand, set on ice, and was pre-run in 0.5X TBE for 1 hr at 200 V. Six µL of the PCR product with amplified *p53* DNA binding domain and 12 µL of formamide dye loading buffer (Invitrogen, Vilinius, LI) were mixed and put in a hot water bath at 95 °C for 10 min to produce single stranded DNA. The mixture was then chilled in ice for 10 min and was loaded into gel wells for vertical gel electrophoresis. The gel electrophoresis was run at 72 V for 3 hr with the gel apparatus submerged in ice.

Once the tracking dye ran to the bottom of the casting, the gel was cracked open, removed, and then immersed in 500 mL of 10% acetic acid and shaken for 60 min on an oscillatory shaker. Acetic acid was subsequently decanted and was replaced with 500 mL of distilled water. The gel was shaken for another 20 min to allow the dye to dissipate from the gel

and the water was decanted. Next, the gel was stained with 1x SYBR Gold Nucleic Acid Gel stain (Invitrogen, S11494) by adding 1 µL of stain into 50 mL of deionized water. This dilute stain was then added to the tray and shaken for another 30 min. The gel was then viewed on a UV transilluminator (Proteinsimple, Santa Clara, CA, USA) to reveal the DNA band pattern which indicates polymorphism of the amplified P53 DNA binding domain.

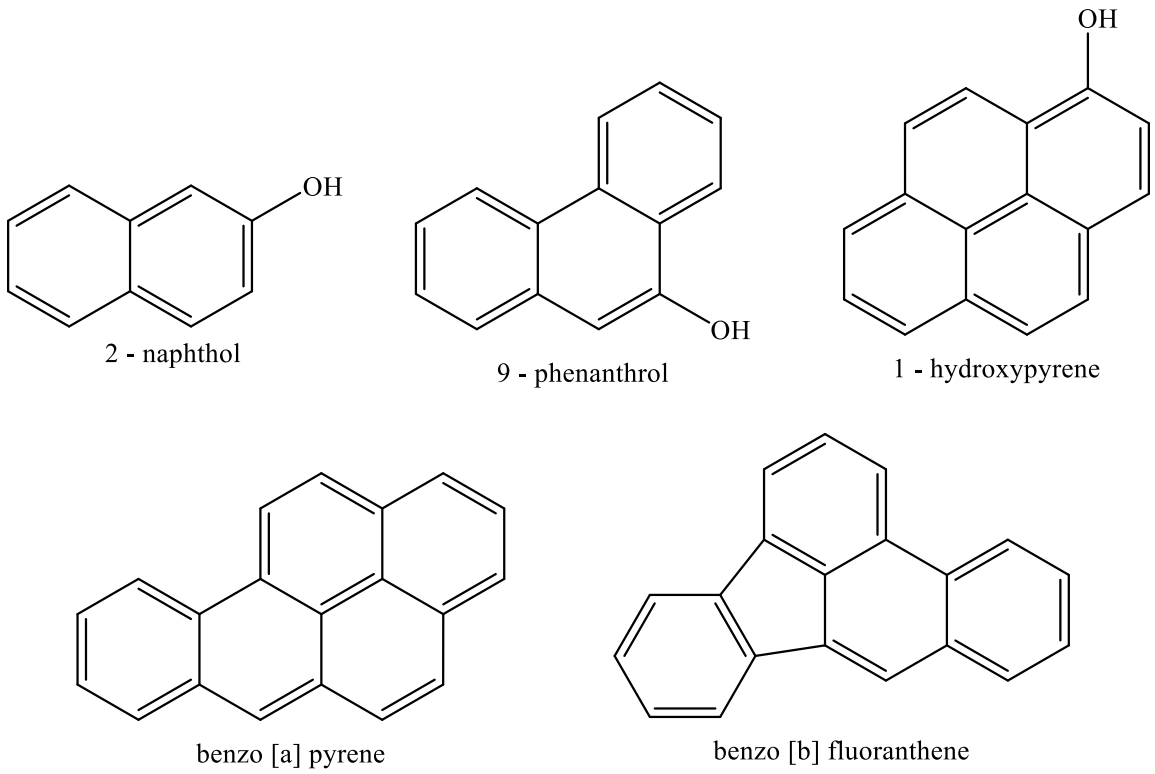

Figure 4: Structures of aromatic standards. Derived from ChemDraw (license by Seton Hall University libraries)

Results

Coastline Area	Date Collected	Samples	Tissues	Fish Weight (g)	Fish Length (cm)
VBLA	8/16/2013	270	L,M,H	135.0	19.0
		271	H,G,L	133.2	18.5
		272	M,L,G,H	215.0	19.4
		276	G,L,M,H	137.0	19.5
		277	G,H	138	19.0
		278	L	139	20.3
		279*	M,D,L,G	195	21.5
	6/8/2013	291*	G,L,M,H	168	19.0
		295	G,L,M,H	112.0	18.0
		300*	L	197	19.5
		302*	L,M	189	19.5
		305*	L,M	218	21.5
GILA	9/11/12	420	G,L,D	137.0	19.0
		413*	D	152.0	18.3
		422*	L	105.6	17.7
		423*	L	94.3	16.4
	6/20/13	520	L	55	14.8
		521*	L,M,G,H	61	16.8
		524	L	54	15.0
		526*	L	139	19
		527	L	101	17.1
		531	L	53	137
		532*	L,M	58	17.3
		533*	L,M	68	15.6
		534*	L,M	55	16.8
	8/19/13	554	L,G	50	15.0
		556*	H	43.5	13.0
		560	L,G,D,H,M	46	15.1
		562*	LM	31	11.5
		564*	L	36	12.2

Table 2: Gulf menhaden sample identification, date collection and average weight and length

* indicate fish that were dissected but did not have fluorescence analysis data collected.

Standard Analysis

Multiple PAH standards were analyzed by EEMs to determine what types of PAH-like compounds were present in the fish organs. PAH standards show different EEM patterns which are distinctly correlated with an individual PAH. The PAH standards analyzed were 2-naphthol-, 9- phenanthrol, 1-hydroxypyrene, benzo[a]pyrene, and benzo[b]fluoranthene. 2-Naphthol is a two-fused aromatic ring molecule associated with a hydroxyl group at the C-2 position. 9-Phenanthrol is a three fused aromatic ring molecule with a hydroxyl group at the C-9 position. 1-Hydroxypyrene is a four fused aromatic ring molecule with a hydroxyl group at the C-1 position. Benzo [a] pyrene, is a five fused aromatic ring molecule with an additional ring added to pyrene. Benzo[b]fluoranthene is also a five fused aromatic ring molecule.

In addition to the PAH standards, multiple biological standards were analyzed by EEMs to differentiate and determine what types of compounds were present in the fish organs. A wide variety of compounds are capable of yielding fluorescence signals. Some relevant naturally occurring biological fluorophores include albumin, vitamin E, vitamin A, and nicotinamide adenine dinucleotide (NADH). Albumin is a simple protein that is soluble in water which contains the fluorescent amino acids tryptophan and tyrosine. Vitamin E and vitamin A are hydrophobic compounds associated with fish livers as well as other organs. Note, this standard data was obtained by previous graduate students in the lab (see DeFelice; Pena; Ridley). All EEMs spectra are shown below, with the intensity of fluorescence indicated by the color legend in units of cps/mV (S1/R1). All spectra were corrected for background, blank, lamp intensity variations and photomultiplier tube nonlinearities.

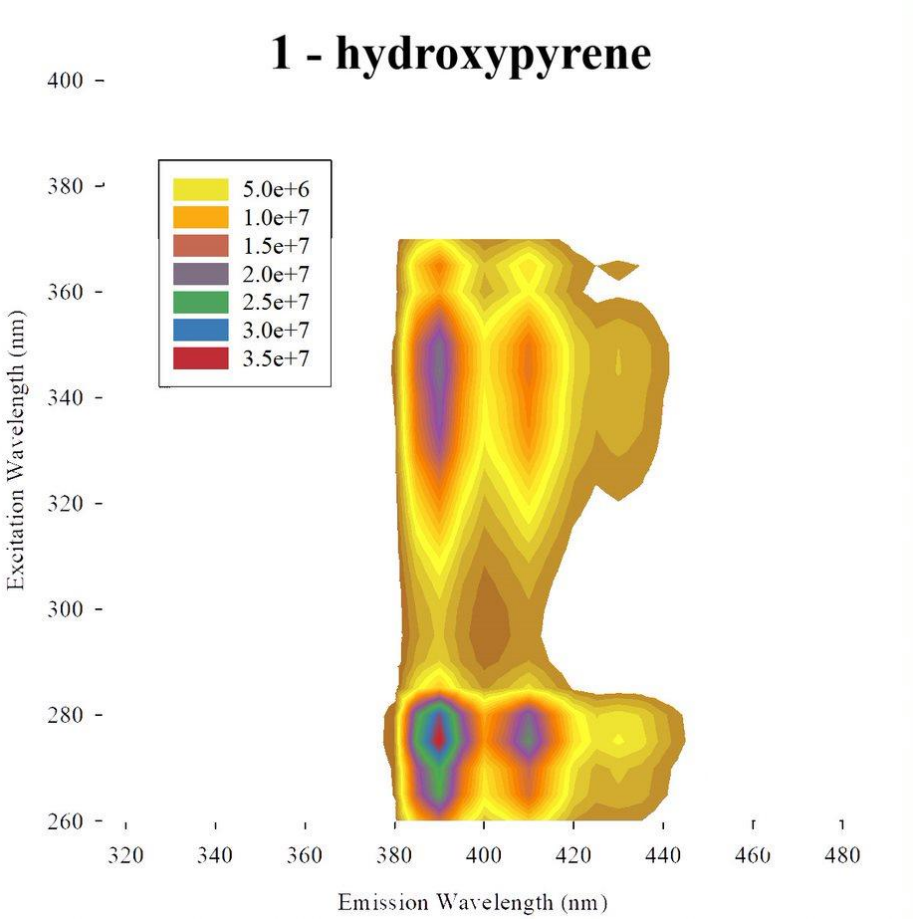

Figure 5: EEM spectrum of PAH standard 1-hydroxypyrene in 75% ethanol.

The EEM spectrum of 1-hydroxypyrene can be seen in Figure 5 at a concentration of 0.02 µg/mL. The excitation spectrum is observed between wavelengths 260 and 360 nm and the emission spectrum is observed between wavelengths 380-430 nm. Two maximal signals can be seen. The first at an excitation wavelength of 270 nm and an emission wavelength of 390 nm. The second maximal signal can be seen at an excitation wavelength of 330 nm and an emission wavelength of 410 nm.

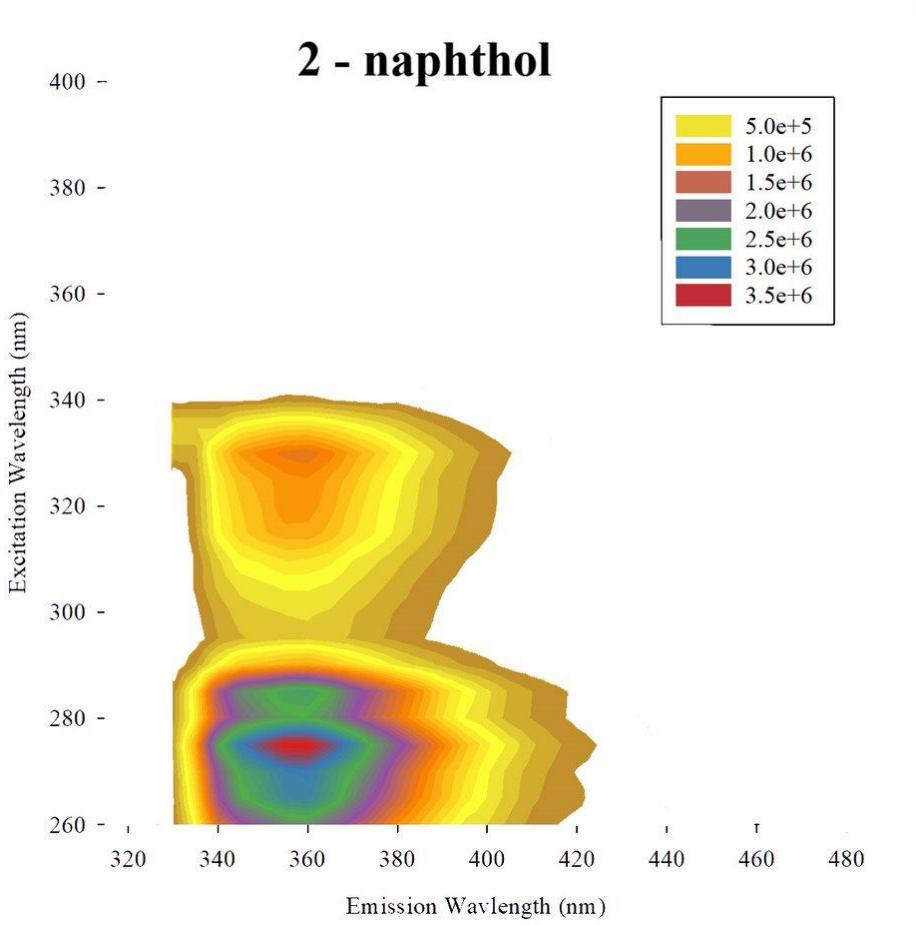

Figure 6: EEM spectrum of PAH standard 2- naphthol in 75% ethanol.

The EEM spectrum of 2- naphthol can be seen in Figure 6 at a concentration of 0.2 µg/mL. The excitation spectrum is observed between wavelengths 260 and 340 nm and the emission spectrum is observed between wavelengths 325-420 nm. Two maximal signals can be seen. The first at an excitation wavelength of 275 nm and an emission wavelength of 345 nm. The second maximal signal can be seen at an excitation wavelength of 325 nm and an emission wavelength of 350 nm.

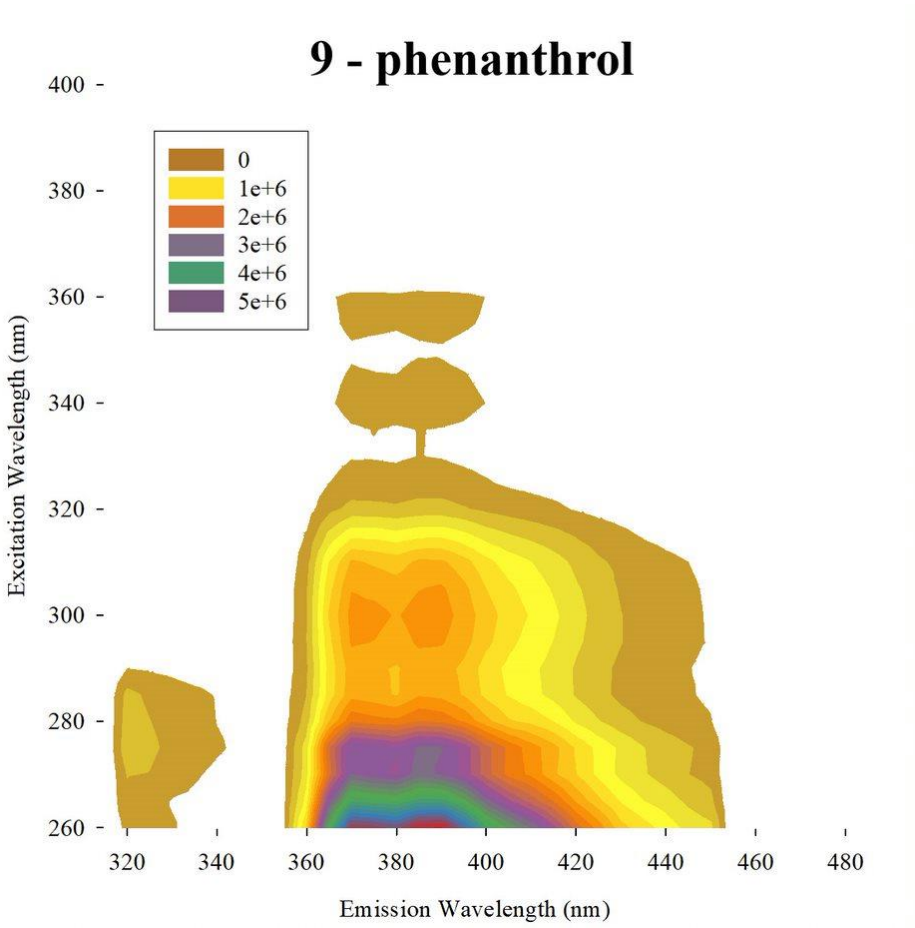

Figure 7: EEM spectrum of PAH standard 9- phenanthrol in 75% ethanol.

The EEM spectrum of 9- phenanthrol can be seen in Figure 7 at a concentration of 0.3 µg/mL. The excitation spectrum is observed between wavelengths 260 and 360 nm and the emission spectrum is observed between wavelengths 320-450 nm. One maximal signal can be seen at an excitation wavelength of 260 nm and an emission wavelength of 380 nm.

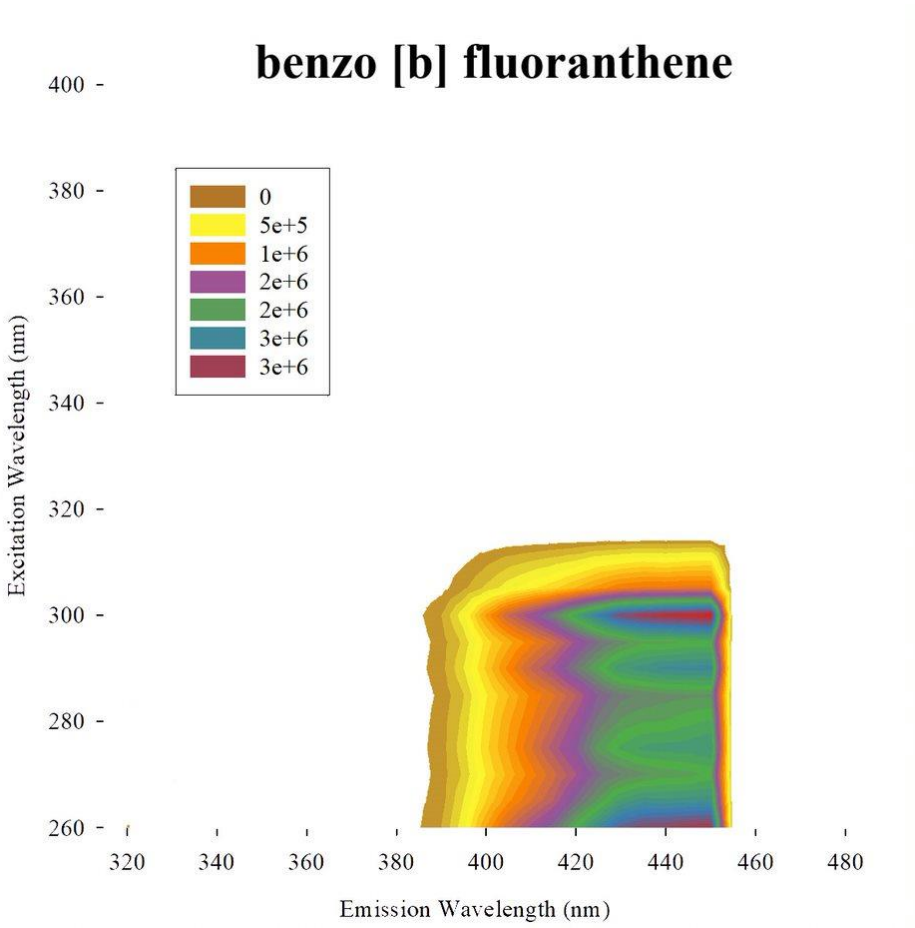

Figure 8: EEM spectrum of PAH standard benzo[b] fluoranthene extracted in 75% ethanol.

The EEM spectrum of benzo[b] fluoranthene can be seen in Figure 8 at a concentration of 0.3 µg/mL. The excitation spectrum is observed between wavelengths 260 and 310 nm and the emission spectrum is observed between wavelengths 385-455 nm. One maximal signal can be seen at an excitation wavelength of 260 nm and an emission wavelength of 415 nm.

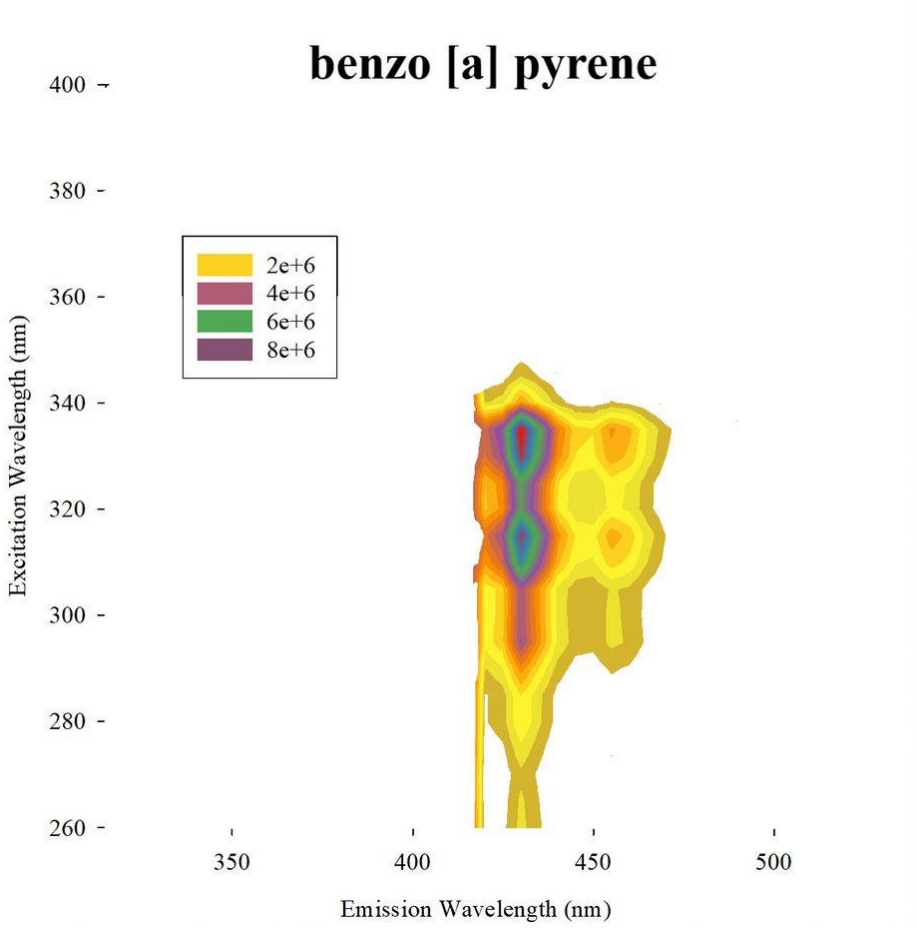

Figure 9: EEM spectrum of PAH standard benzo [a] pyrene extracted in 75% ethanol.

The EEM spectrum of benzo [a] pyrene can be seen in Figure 9 at a concentration of 0.06 µg/mL. The excitation spectrum is observed between wavelengths 260 and 345 nm and the emission spectrum is observed between wavelengths 410-455 nm. Two maximal signals can be seen. The first at an excitation wavelength of 310 and an emission wavelength of 430 nm. The second maximal signal can be seen at an excitation wavelength of 330 nm and an emission wavelength of 430 nm.

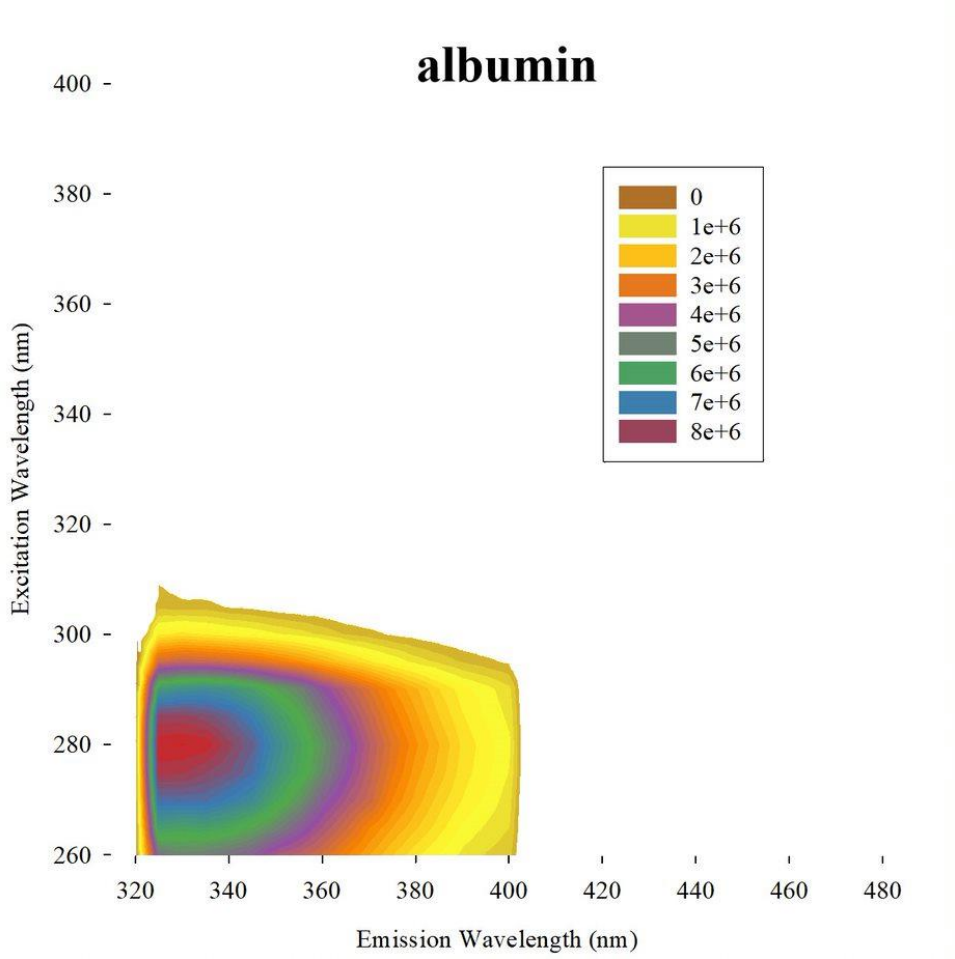

Figure 10: EEM spectrum of biological standard albumin extracted in 75% ethanol.

The EEM spectrum of albumin can be seen in Figure 10 at a concentration of 1000 ng/mL. The excitation spectrum is observed between wavelengths 260 and 310 nm and the emission spectrum is observed between wavelengths 320-400 nm. One maximal signal can be seen at an excitation wavelength of 280 nm and an emission wavelength of 330 nm.

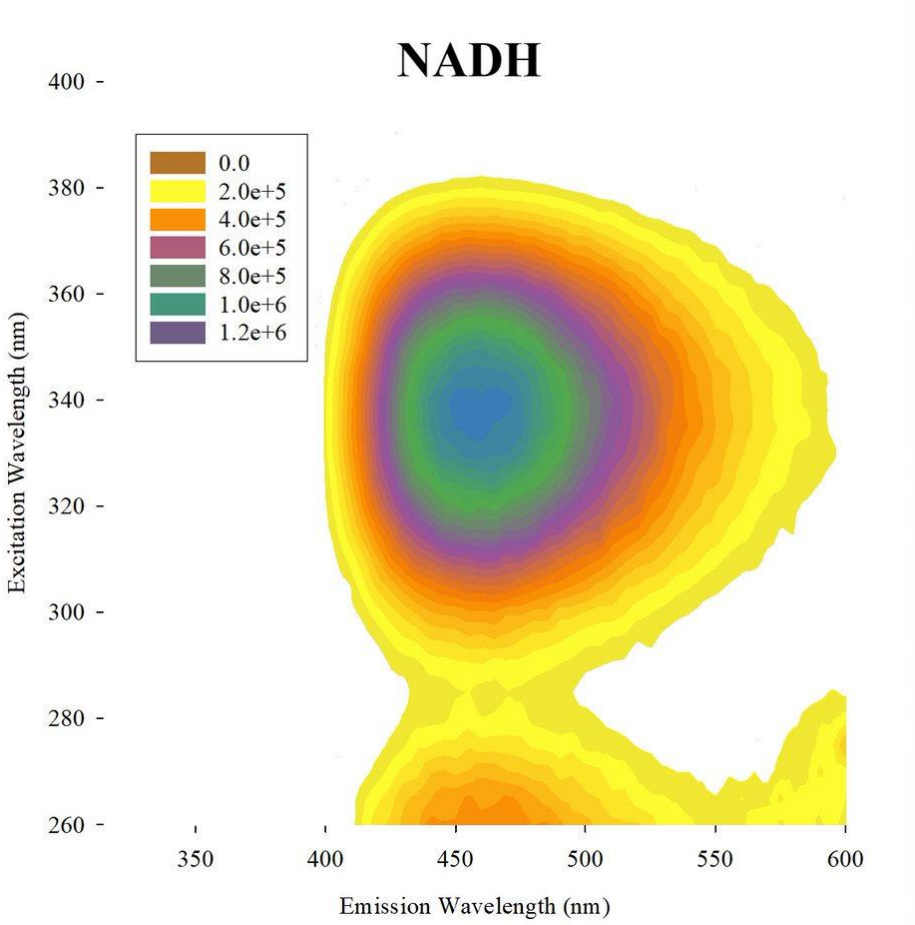

Figure 11: EEM spectrum of biological standard NADH in 75% ethanol.

The EEM spectrum of NADH can be seen in Figure 11 at a concentration of 100,000 ng/mL. The excitation spectrum is observed between wavelengths 260 and 380 nm and the emission spectrum is observed between wavelengths 410-600 nm. One maximal signal can be seen at an excitation wavelength of 340 nm and an emission wavelength of 450 nm.

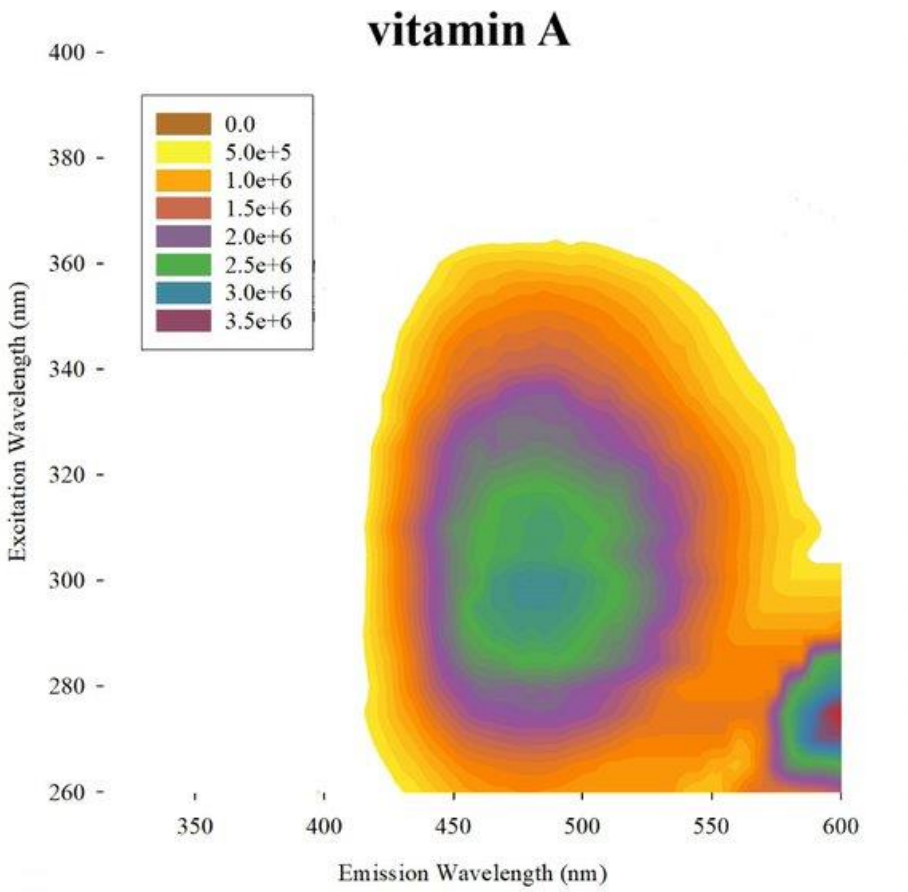

Figure 12: EEM spectrum of biological standard vitamin A in 75% ethanol.

The EEM spectrum of vitamin A can be seen in Figure 12 at a concentration of 25,000 ng/mL. The excitation spectrum is observed between wavelengths 260 and 360 nm and the emission spectrum is observed between wavelengths 420-600 nm. Two maximal signals can be seen. The first at an excitation wavelength of 320 nm and an emission wavelength of 480 nm. The second maximal signal can be seen at an excitation wavelength of 275 nm and an emission wavelength of 600 nm.

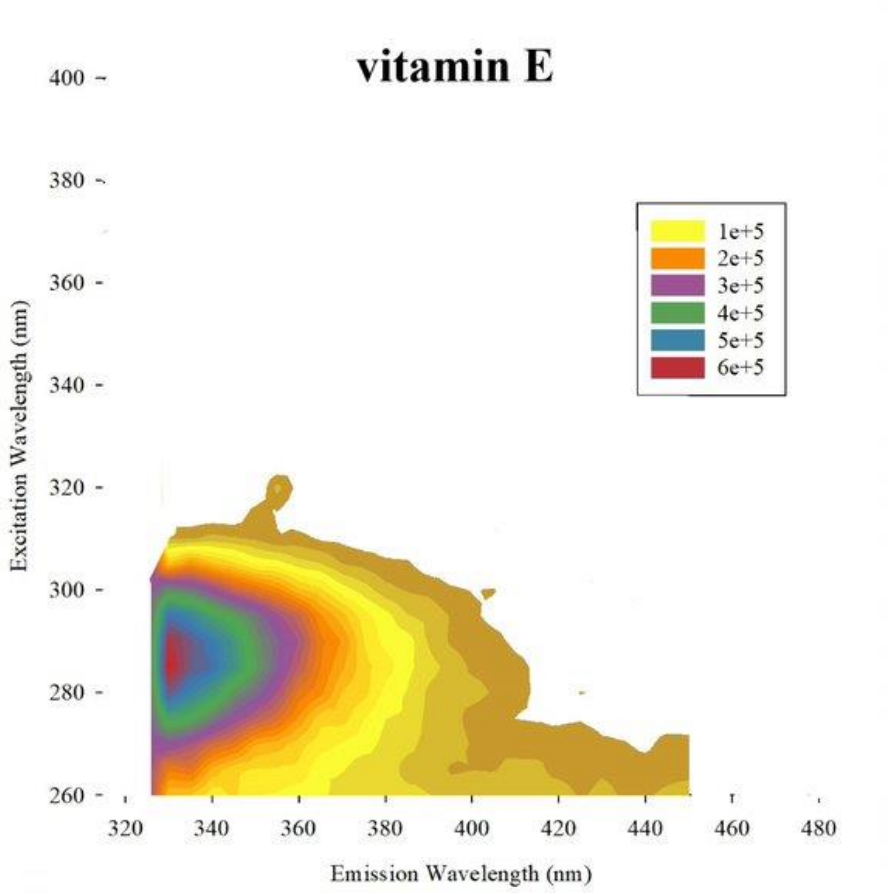

Figure 13: EEM spectrum of biological standard vitamin E in 75% ethanol.

The EEM spectrum of vitamin E can be seen in Figure 13 at a concentration of 5,000 ng/mL. The excitation spectrum is observed between wavelengths 260 and 315 nm and the emission spectrum is observed between 320-450 nm. One maximal signal can be seen at an excitation wavelength of 290 nm and an emission wavelength of 325 nm.

Ingestion and metabolism of PAH compounds was determined via EEM measurements of fish organ extracts. **Figure 14** illustrates an EEM scan of raw crude oil obtained from the GOM. The raw crude oil excitation spectrum is observed between wavelengths 280-360 nm and the emission spectrum is observed between 320-420 nm. One maximal signal can be seen at an excitation wavelength of 300 nm and an emission wavelength of 360 nm.

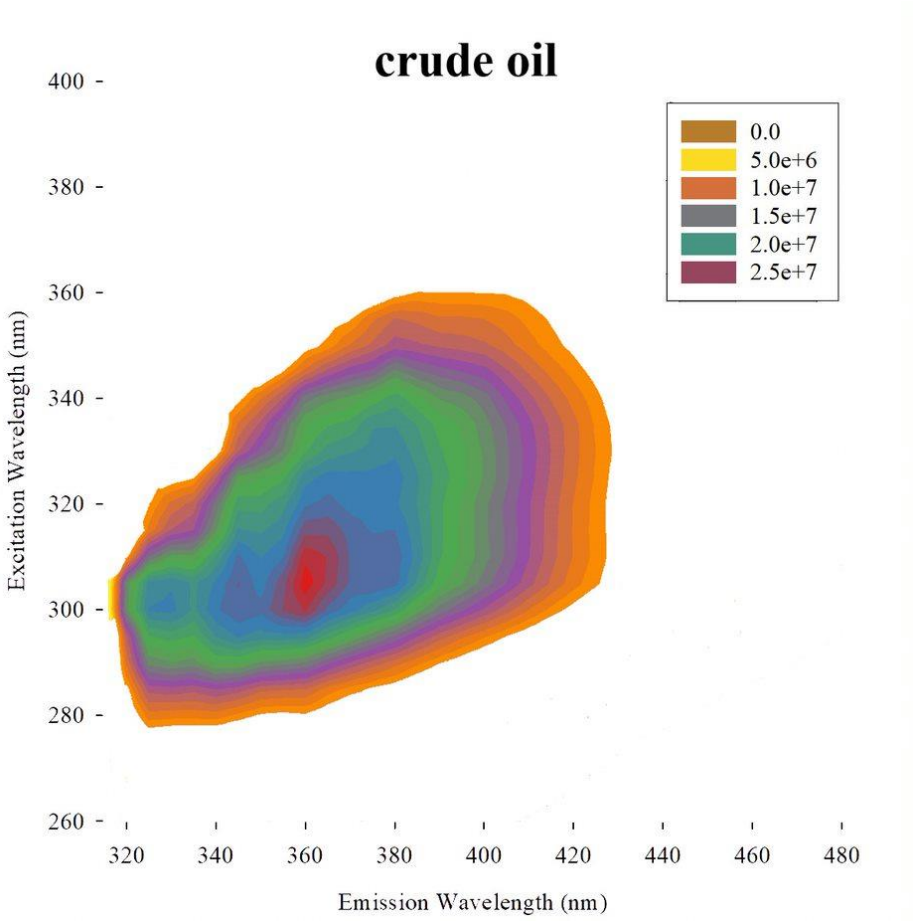

Figure 14: EEM spectrum of raw crude oil from the Gulf of Mexico in 1 mL of 75% ethanol.

The EEM spectrum of raw crude oil can be seen in Figure 14 at a concentration of 5µL. The excitation spectrum is observed between wavelengths 280-360 nm and the emission spectrum is observed between 320-420 nm. One maximal signal can be seen at an excitation wavelength of 300 nm and an emission wavelength of 360 nm.

The GILA samples analyzed consisted of 420 D, 420 G, 420 L, 520 L, 527 L, 531 L, 554 L, and 560 L. The VBLA samples analyzed consisted of 270 L, 271 H, 271 G, 271 L, 272 L, 276 G, 276 H, 276 L, 276 M, 277 G, 277 H, 278 L, 295 G, and 295 L.

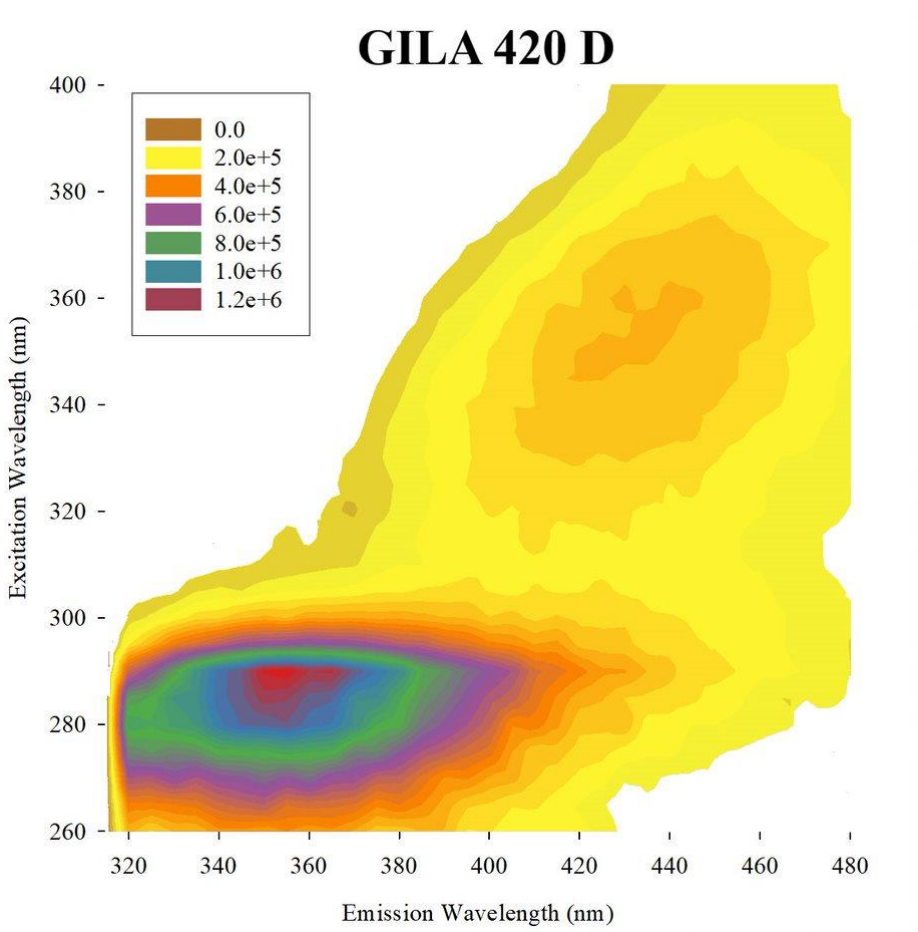

Figure 15: EEM spectrum of GILA 420 gonad extracted in 1 mL of 75% ethanol.

The EEM spectrum of GILA 420 D can be seen in Figure 15. The excitation spectrum is observed between wavelengths 260-400 nm and the emission spectrum is observed between wavelengths 320-480 nm. Two maximal signals can be seen. One at an excitation wavelength of 290 nm and an emission wavelength of 350 nm. This peak is comparable to that of raw crude oil that has a maximum peak at an excitation wavelength of 300 nm and an emission wavelength of 360 nm. The second maximal signal can be seen at an excitation wavelength of 350 nm and an emission wavelength of 430 nm. This peak is comparable to that of 1- hydroxypyrene that has a maximum peak at an excitation wavelength of 345 nm and an emission wavelength of 410 nm.

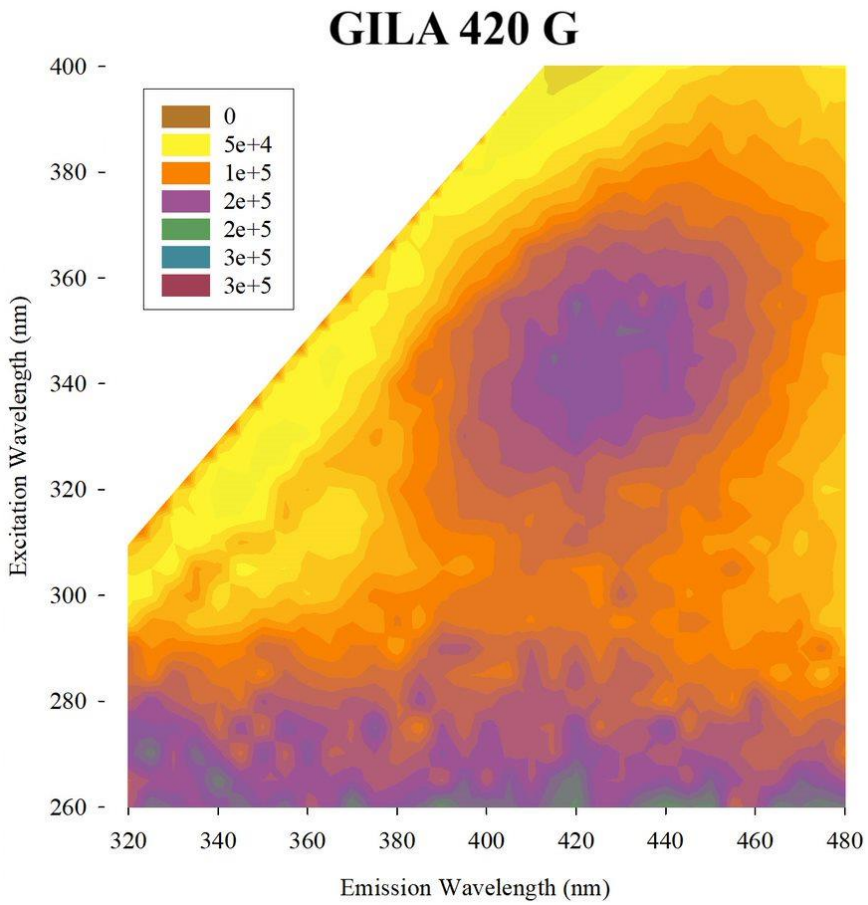

Figure 16: EEM spectrum of GILA 420 gill extracted in 1 mL of 75% ethanol.

The EEM spectrum of GILA 420 G can be seen in Figure 16. The excitation spectrum is observed between wavelengths 260-400 nm and the emission spectrum is observed between wavelengths 320-480 nm. One maximal signal can be seen at an excitation wavelength of 300 nm and an emission wavelength of 360 nm. This peak is comparable to that of raw crude oil that has a maximum peak at an excitation wavelength of 300 nm and an emission wavelength of 360 nm.

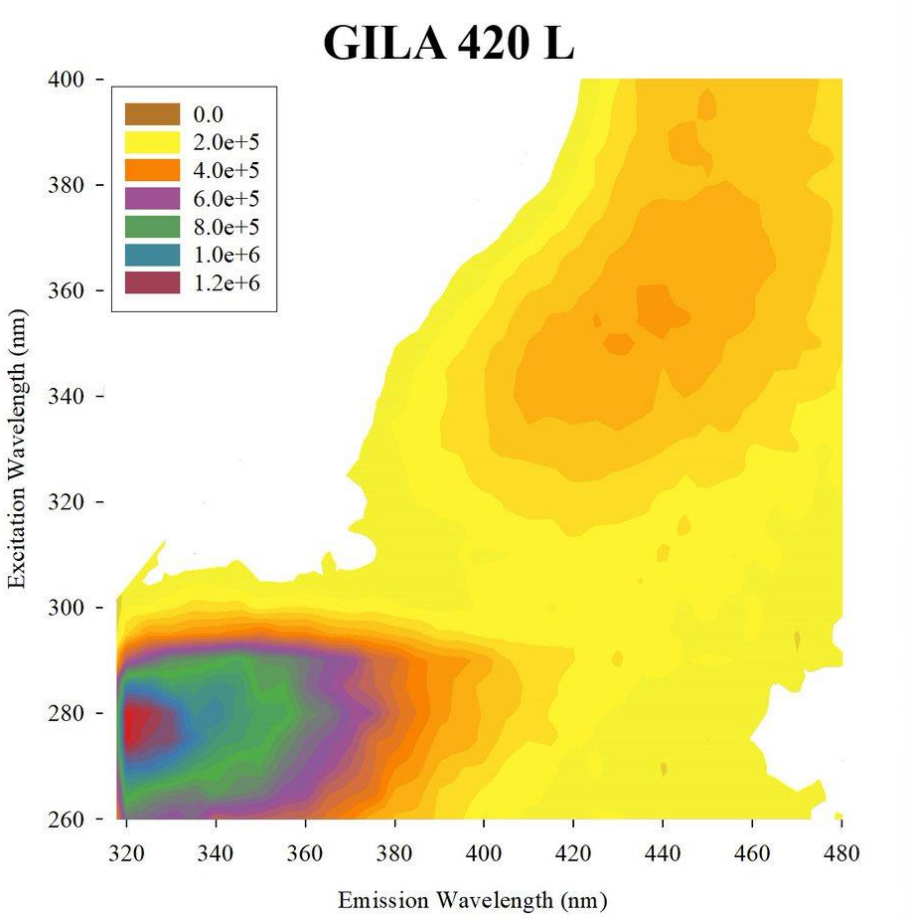

Figure 17: EEM spectrum of GILA 420 liver extracted in 1 mL of 75% ethanol.

The EEM spectrum of GILA 420 L can be seen in Figure 17. The excitation spectrum is observed between wavelengths 260-400 nm and the emission spectrum is observed between wavelengths 320-420 nm. Two maximal signals can be seen. One at an excitation wavelength of 280 nm and an emission wavelength of 320 nm. This peak is comparable to that of albumin that has a maximum peak at an excitation wavelength of 280 nm and an emission wavelength of 330 nm. The second maximal signal can be seen at an excitation wavelength of 350 nm and an emission wavelength of 430 nm. This peak is comparable to that of 1- hydroxypyrene that has a maximum peak at an excitation wavelength of 345 nm and an emission wavelength of 410 nm.

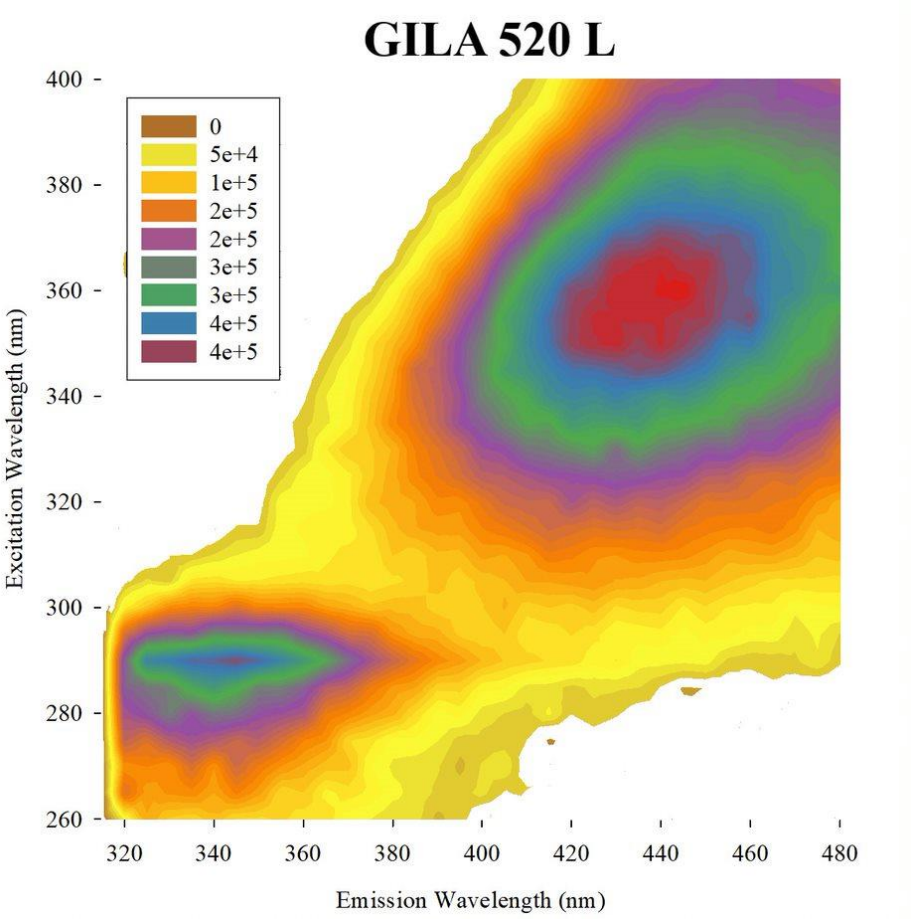

Figure 18: EEM spectrum of GILA 520 liver extracted in 1 mL of 75% ethanol.

The EEM spectrum of GILA 520 L can be seen in Figure 18. The excitation spectrum is observed between wavelengths 260-400 nm and the emission spectrum is observed between wavelengths 315-480 nm. Two maximal signals can be seen. One at an excitation wavelength of 290 nm and an emission wavelength of 350 nm. This peak is comparable to that of raw crude oil that has a maximum peak at an excitation wavelength of 300 nm and an emission wavelength of 360 nm. The second maximal signal can be seen at an excitation wavelength of 350 nm and an emission wavelength of 430 nm. This peak is comparable to that of 1- hydroxypyrene that has a maximum peak at an excitation wavelength of 345 nm and an emission wavelength of 410 nm.

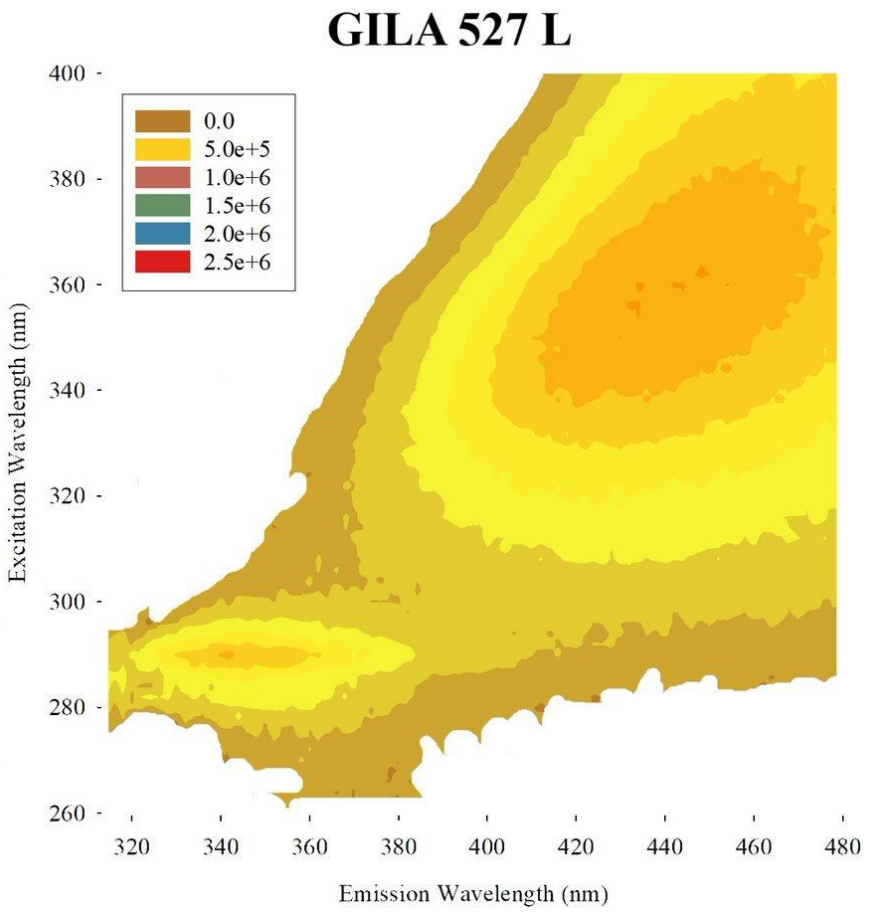

Figure 19: EEM spectrum of GILA 527 liver extracted in 1 mL of 75% ethanol.

The EEM spectrum of GILA 527 L can be seen in Figure 19. The excitation spectrum is observed between wavelengths 260-400 nm and the emission spectrum is observed between wavelengths 315-480 nm. Two maximal signals can be seen. One at an excitation wavelength of 290 nm and an emission wavelength of 350 nm. This peak is comparable to that of raw crude oil that has a maximum peak at an excitation wavelength of 300 nm and an emission wavelength of 360 nm. The second maximal signal can be seen at an excitation wavelength of 360 nm and an emission wavelength of 440 nm. This peak is comparable to that of vitamin A that has a maximum peak at an excitation wavelength of 345 nm and an emission wavelength of 480 nm.

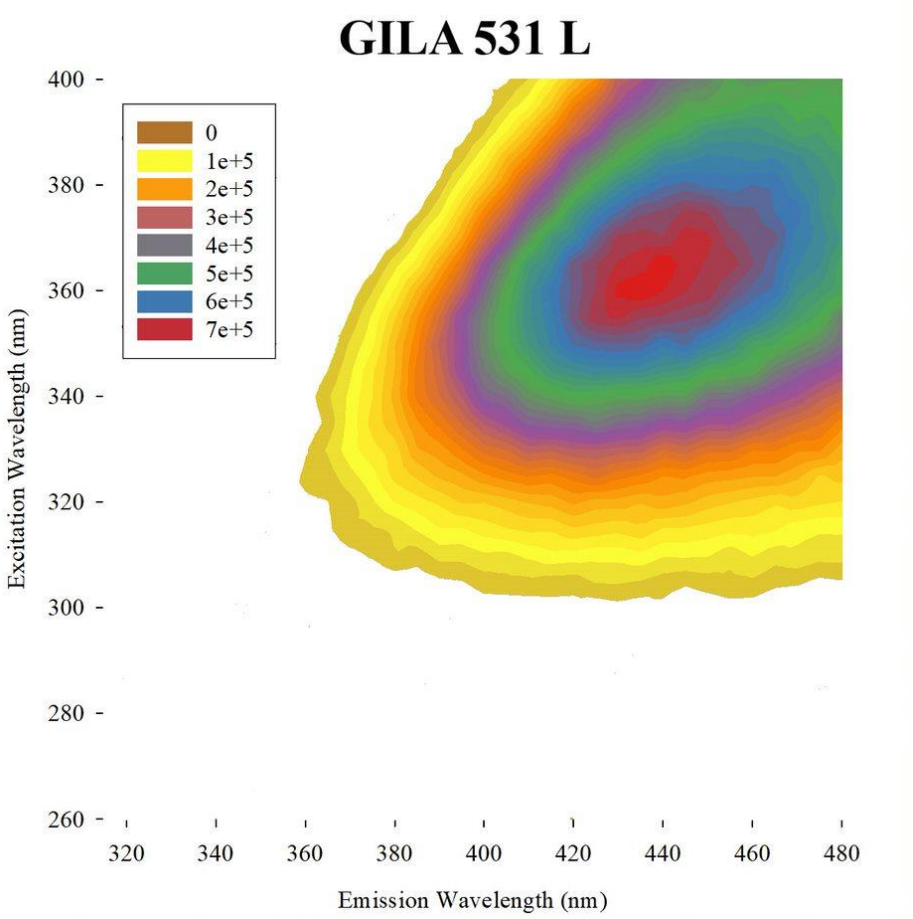

Figure 20: EEM spectrum of GILA 531 liver extracted in 1 mL of 75% ethanol.

The EEM spectrum of GILA 531 L can be seen in Figure 20. The excitation spectrum is observed between wavelengths 300-400 nm and the emission spectrum is observed between wavelengths 360-480 nm. One maximal signal can be seen at an excitation wavelength of 360 nm and an emission wavelength of 430 nm. This peak is comparable to that of 1- hydroxypyrene that has a maximum peak at an excitation wavelength of 345 nm and an emission wavelength of 410 nm.

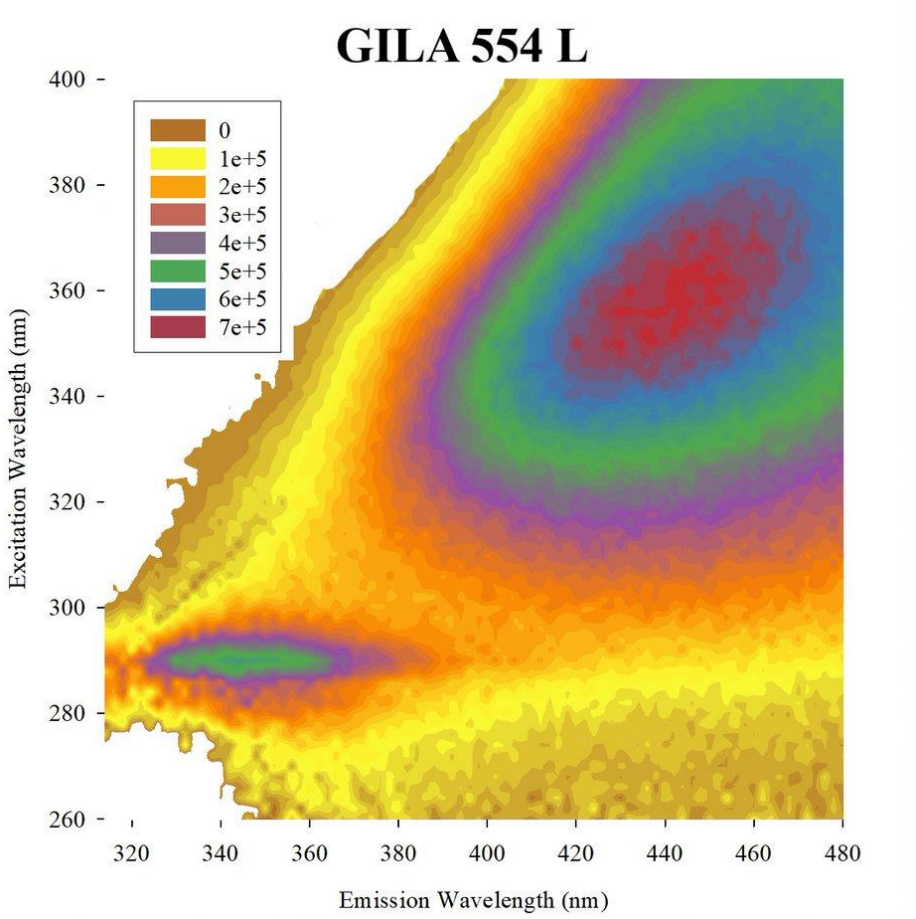

Figure 21: EEM spectrum of GILA 554 liver extracted in 1 mL of 75% ethanol.

The EEM spectrum of GILA 554 L can be seen in Figure 21. The excitation spectrum is observed between wavelengths 260-400 nm and the emission spectrum is observed between wavelengths 315-480 nm. Two maximal signals can be seen. One at an excitation wavelength of 290 nm and an emission wavelength of 350 nm. This peak is comparable to that of raw crude oil that has a maximum peak at an excitation wavelength of 300 nm and an emission wavelength of 360 nm. The second maximal signal can be seen at an excitation wavelength of 350 nm and an emission wavelength of 430 nm. This peak is comparable to that of 1- hydroxypyrene that has a maximum peak at an excitation wavelength of 345 nm and an emission wavelength of 410 nm.

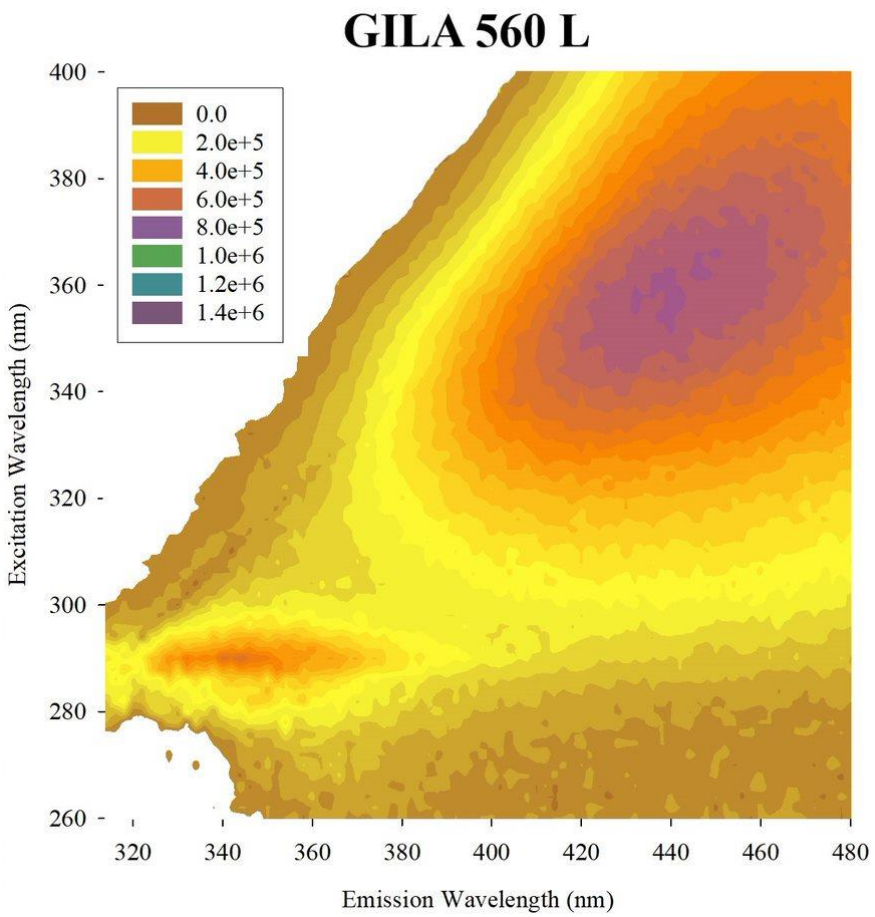

Figure 22: EEM spectrum of GILA 560 liver extracted in 1 mL of 75% ethanol.

The EEM spectrum of GILA 560 L can be seen in Figure 22. The excitation spectrum is observed between wavelengths 260-400 nm and the emission spectrum is observed between wavelengths 315-480 nm. Two maximal signals can be seen. One at an excitation wavelength of 290 nm and an emission wavelength of 350 nm. This peak is comparable to that of raw crude oil that has a maximum peak at an excitation wavelength of 300 nm and an emission wavelength of 360 nm. The second maximal signal can be seen at an excitation wavelength of 350 nm and an emission wavelength of 430 nm. This peak is comparable to that of 1- hydroxypyrene that has a maximum peak at an excitation wavelength of 345 nm and an emission wavelength of 410 nm.

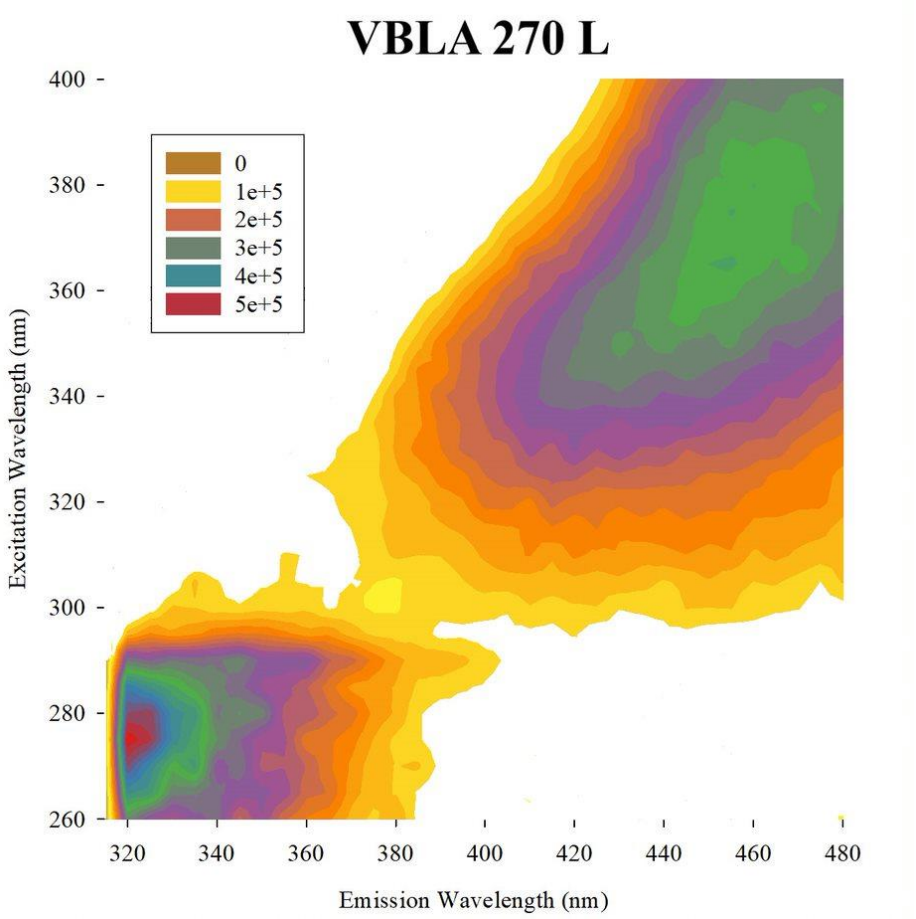

Figure 23: EEM spectrum of VBLA 270 liver extracted in 1 mL of 75% ethanol.

The EEM spectrum of VBLA 270 L can be seen in Figure 23. The excitation spectrum is observed between wavelengths 260-400 nm and the emission spectrum is observed between wavelengths 315-480 nm. Two maximal signals can be seen. One at an excitation wavelength of 290 nm and an emission wavelength of 340 nm. This peak is comparable to that of raw crude oil that has a maximum peak at an excitation wavelength of 300 nm and an emission wavelength of 360 nm. The second maximal signal can be seen at an excitation wavelength of 350 nm and an emission wavelength of 430 nm. This peak is comparable to that of 1- hydroxypyrene that has a maximum peak at an excitation wavelength of 345 nm and an emission wavelength of 410 nm.

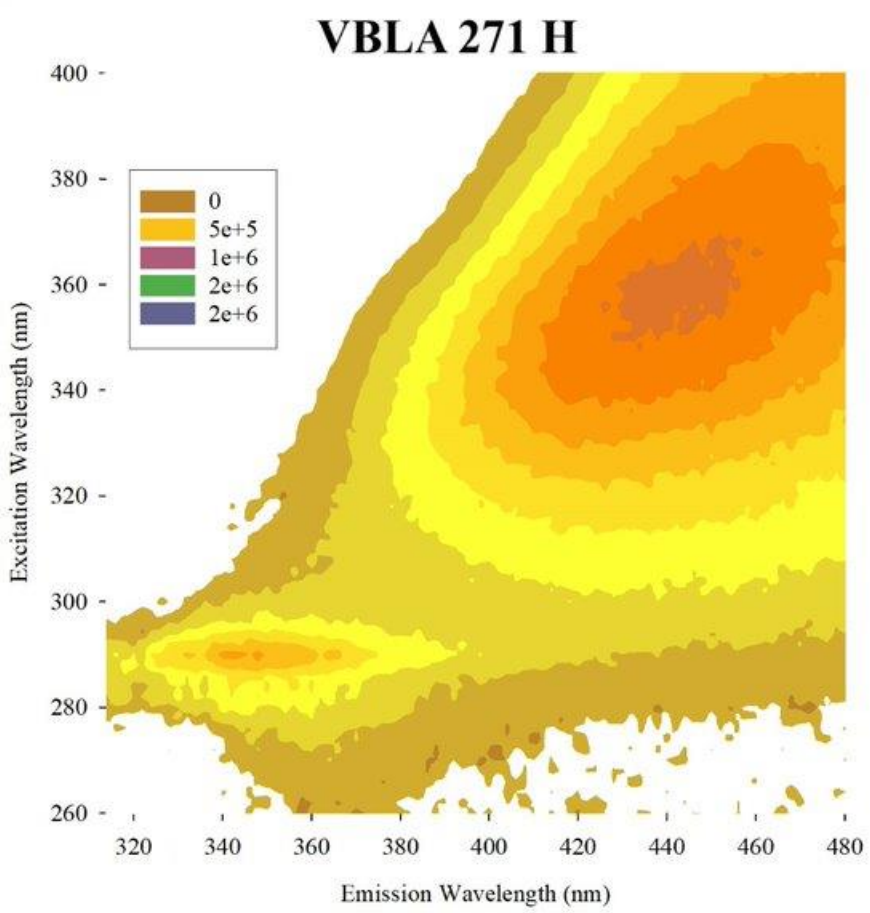

Figure 24: EEM spectrum of VBLA 271 heart extracted in 1 mL of 75% ethanol.

The EEM spectrum of VBLA 271 H can be seen in Figure 24. The excitation spectrum is observed between wavelengths 260-400 nm and the emission spectrum is observed between wavelengths 315-480 nm. Two maximal signals can be seen. One at an excitation wavelength of 290 nm and an emission wavelength of 340 nm. This peak is comparable to that of raw crude oil that has a maximum peak at an excitation wavelength of 300 nm and an emission wavelength of 360 nm. The second maximal signal can be seen at an excitation wavelength of 350 nm and an emission wavelength of 430 nm. This peak is comparable to that of 1- hydroxypyrene that has a maximum peak at an excitation wavelength of 345 nm and an emission wavelength of 410 nm.

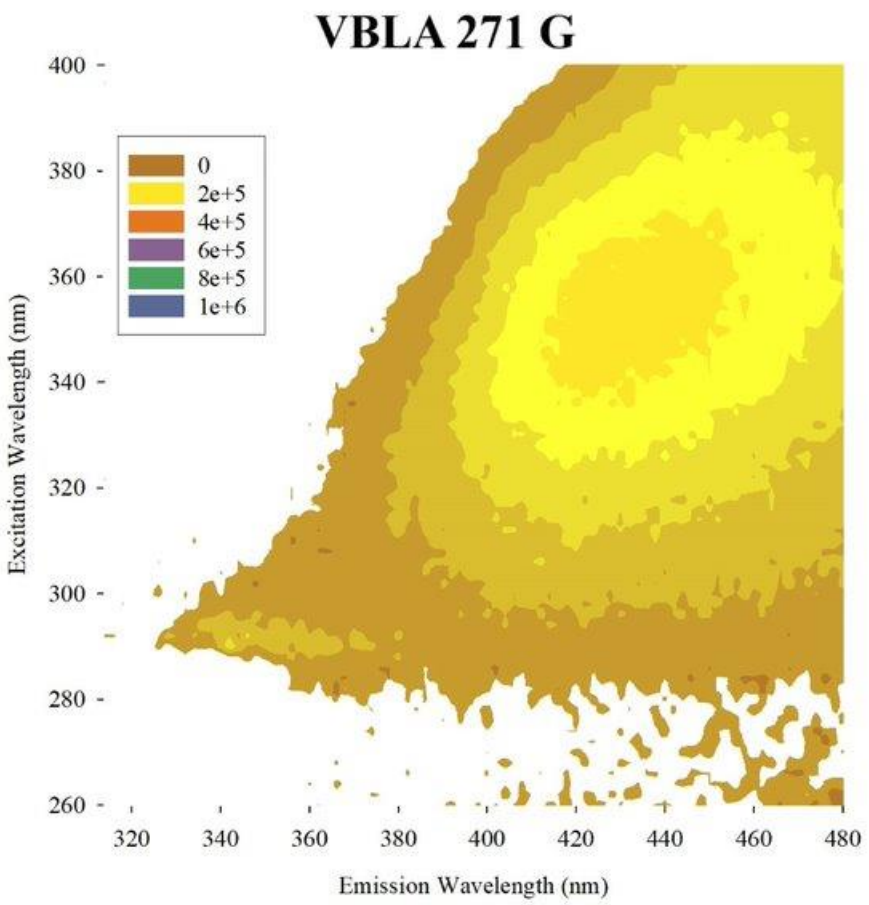

Figure 25: EEM spectrum of VBLA 271 gill extracted in 1 mL of 75% ethanol.

The EEM spectrum of VBLA 271 G can be seen in Figure 25. The excitation spectrum is observed between wavelengths 300-400 nm and the emission spectrum is observed between wavelengths 360-480 nm. One maximal signal can be seen at an excitation wavelength of 360 nm and an emission wavelength of 430 nm. This peak is comparable to that of 1- hydroxypyrene that has a maximum peak at an excitation wavelength of 345 nm and an emission wavelength of 410 nm.

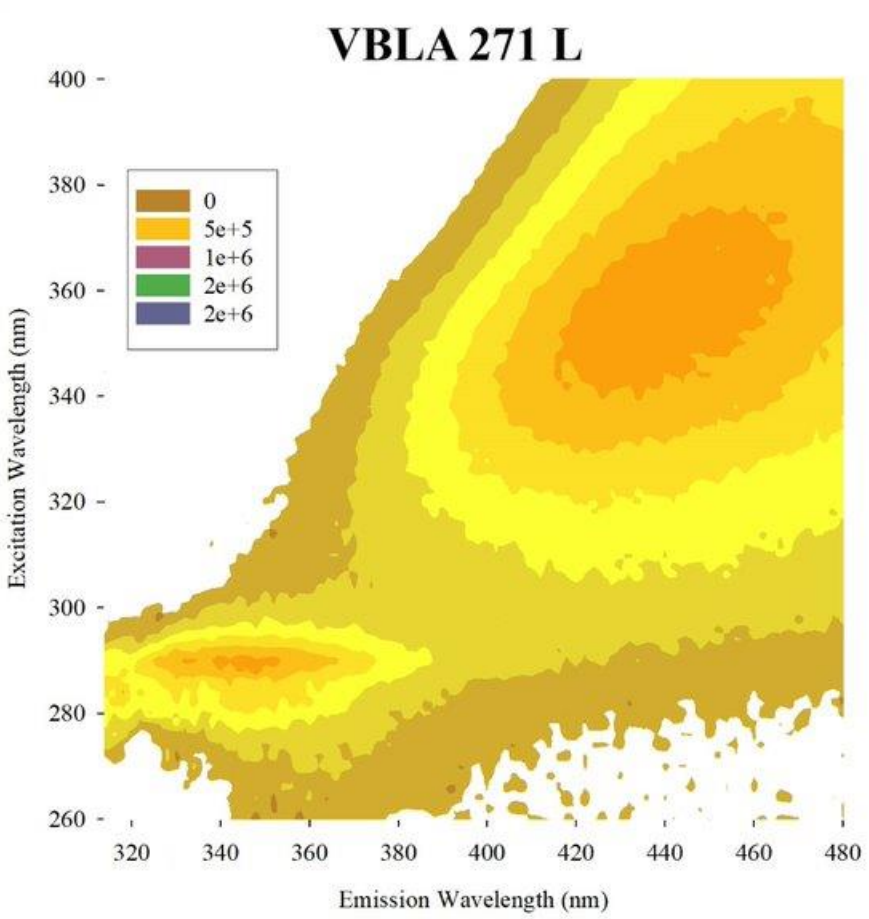

Figure 26: EEM spectrum of VBLA 271 liver extracted in 1 mL of 75% ethanol.

The EEM spectrum of VBLA 271 L can be seen in Figure 26. The excitation spectrum is observed between wavelengths 260-400 nm and the emission spectrum is observed between wavelengths 315-480 nm. Two maximal signals can be seen. One at an excitation wavelength of 290 nm and an emission wavelength of 350 nm. This peak is comparable to that of raw crude oil that has a maximum peak at an excitation wavelength of 300 nm and an emission wavelength of 360 nm. The second maximal signal can be seen at an excitation wavelength of 350 nm and an emission wavelength of 430 nm. This peak is comparable to that of 1- hydroxypyrene that has a maximum peak at an excitation wavelength of 345 nm and an emission wavelength of 410 nm.

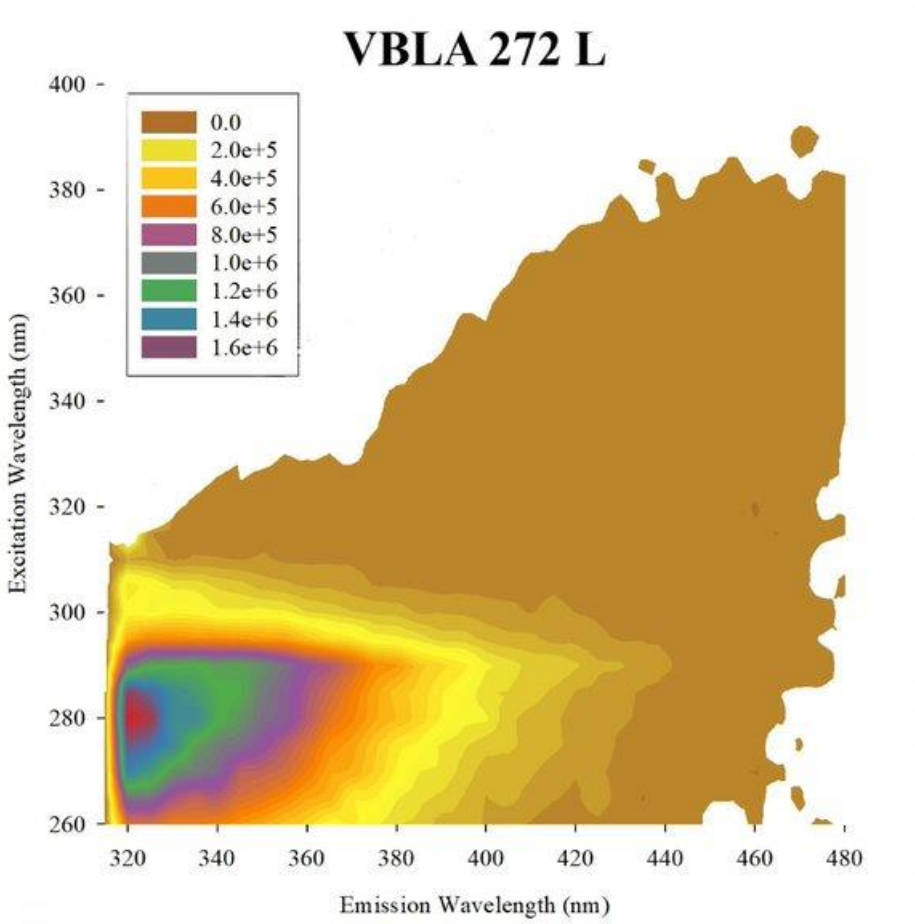

Figure 27: EEM spectrum of VBLA 272 liver extracted in 1 mL of 75% ethanol.

The EEM spectrum of VBLA 272 L can be seen in Figure 27. The excitation spectrum is observed between wavelengths 260-400 nm and the emission spectrum is observed between wavelengths 315-480 nm. One maximal signal can be seen at an excitation wavelength of 290 nm and an emission wavelength of 340 nm. This peak is comparable to that of raw crude oil that has a maximum peak at an excitation wavelength of 300 nm and an emission wavelength of 360 nm.

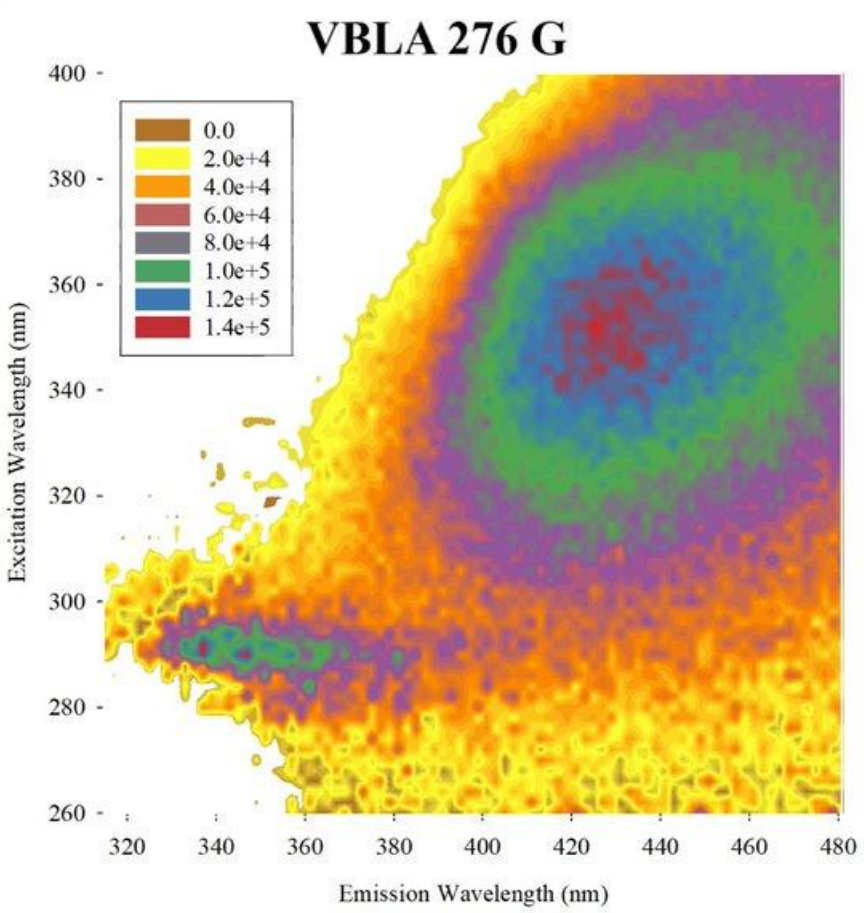

Figure 28: EEM spectrum of VBLA 276 gill extracted in 1 mL of 75% ethanol.

The EEM spectrum of VBLA 276 G can be seen in Figure 28. The excitation spectrum is observed between wavelengths 260-400 nm and the emission spectrum is observed between wavelengths 315-480 nm. Two maximal signals can be seen. One at an excitation wavelength of 290 nm and an emission wavelength of 350 nm. This peak is comparable to that of raw crude oil that has a maximum peak at an excitation wavelength of 300 nm and an emission wavelength of 360 nm. The second maximal signal can be seen at an excitation wavelength of 350 nm and an emission wavelength of 430 nm. This peak is comparable to that of 1- hydroxypyrene that has a maximum peak at an excitation wavelength of 345 nm and an emission wavelength of 410 nm.

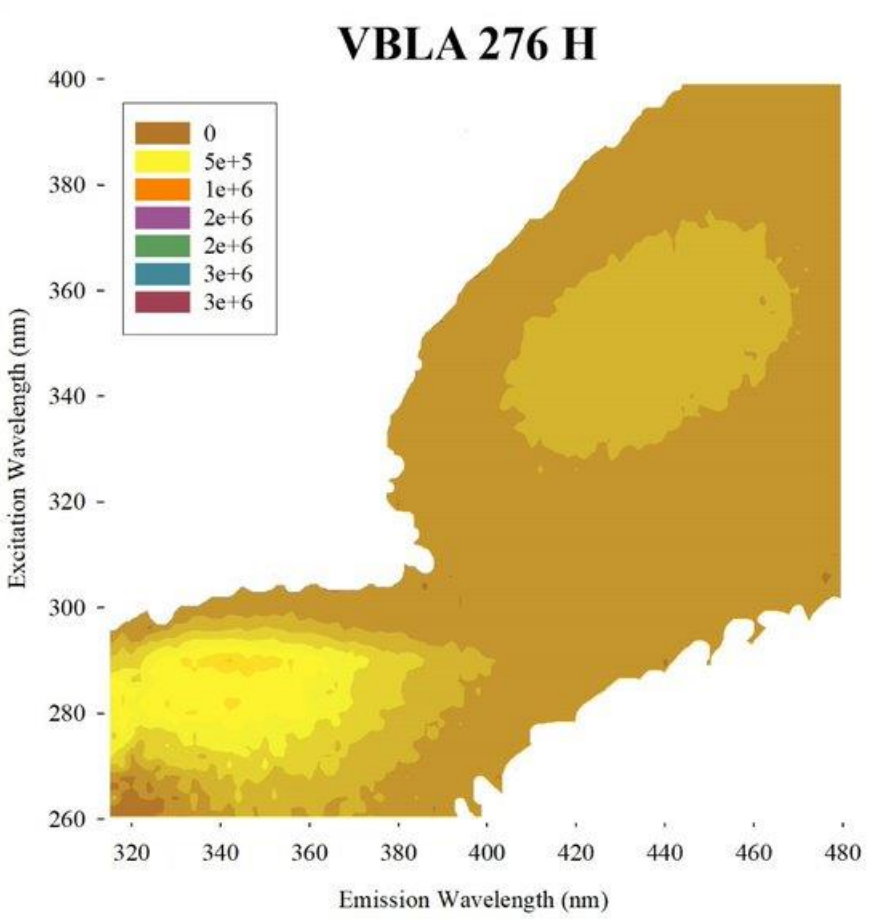

Figure 29: EEM spectrum of VBLA 276 heart extracted in 1 mL of 75% ethanol.

The EEM spectrum of VBLA 276 H can be seen in Figure 29. The excitation spectrum is observed between wavelengths 260-400 nm and the emission spectrum is observed between wavelengths 315-480 nm. Two maximal signals can be seen. One at an excitation wavelength of 290 nm and an emission wavelength of 350 nm. This peak is comparable to that of raw crude oil that has a maximum peak at an excitation wavelength of 300 nm and an emission wavelength of 360 nm. The second maximal signal can be seen at an excitation wavelength of 350 nm and an emission wavelength of 430 nm. This peak is comparable to that of 1- hydroxypyrene that has a maximum peak at an excitation wavelength of 345 nm and an emission wavelength of 410 nm.

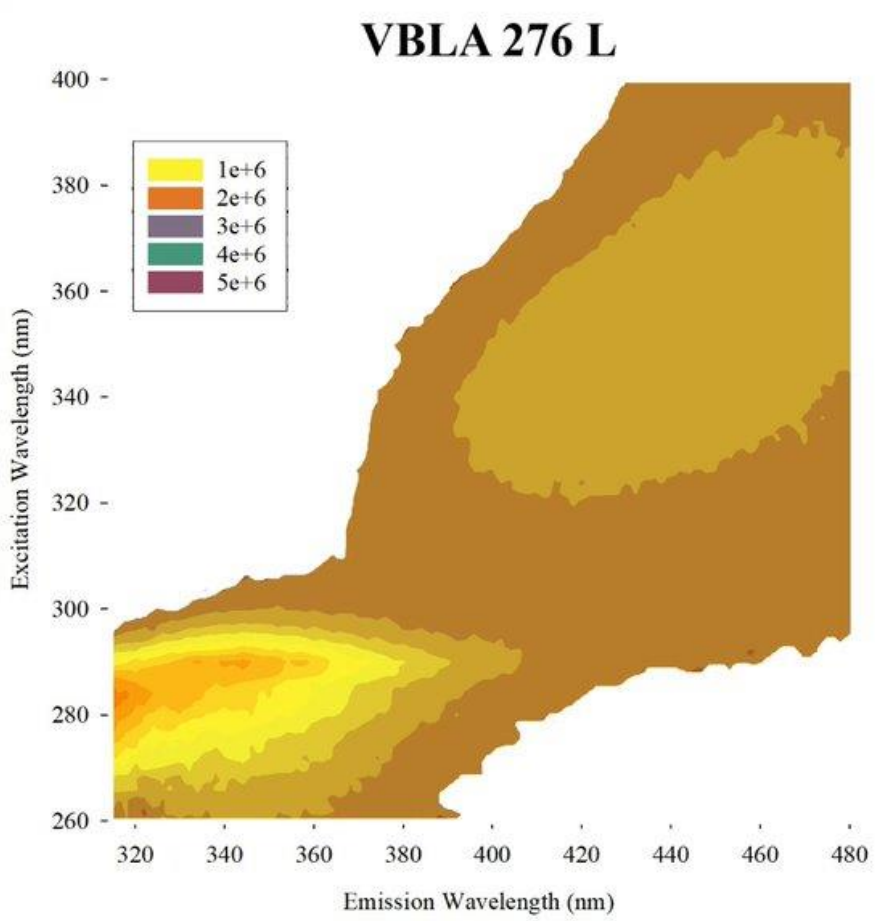

Figure 30: EEM spectrum of VBLA 276 liver extracted in 1 mL of 75% ethanol.

The EEM spectrum of VBLA 276 L can be seen in Figure 30. The excitation spectrum is observed between wavelengths 260-400 nm and the emission spectrum is observed between wavelengths 315-480 nm. Two maximal signals can be seen. One at an excitation wavelength of 290 nm and an emission wavelength of 350 nm. This peak is comparable to that of raw crude oil that has a maximum peak at an excitation wavelength of 300 nm and an emission wavelength of 360 nm. The second maximal signal can be seen at an excitation wavelength of 350 nm and an emission wavelength of 430 nm. This peak is comparable to that of 1- hydroxypyrene that has a maximum peak at an excitation wavelength of 345 nm and an emission wavelength of 410 nm.

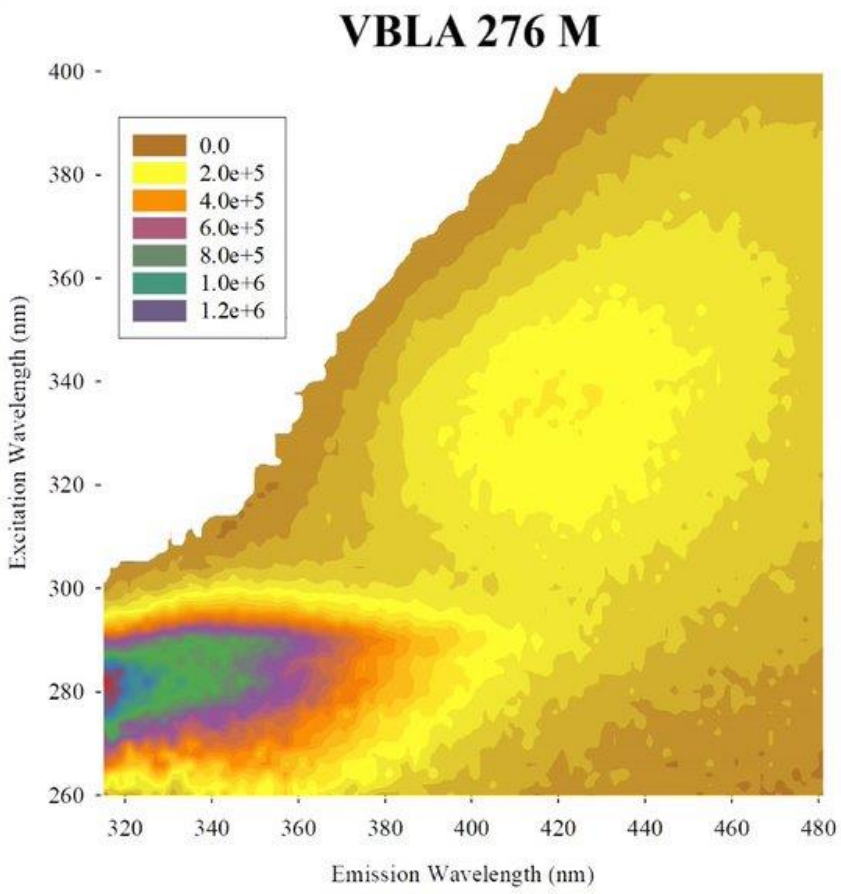

Figure 31: EEM spectrum of VBLA 276 muscle extracted in 1 mL of 75% ethanol.

The EEM spectrum of VBLA 276 M can be seen in Figure 31. The excitation spectrum is observed between wavelengths 260-400 nm and the emission spectrum is observed between wavelengths 315-480 nm. Two maximal signals can be seen. The first at an excitation wavelength of 290 nm and an emission wavelength of 340 nm. This peak is comparable to that of crude oil that has a maximum peak at an excitation wavelength of 290 nm and an emission wavelength of 360 nm. The second maximal signal can be seen at an excitation wavelength of 340 nm and an emission wavelength of 430 nm. This peak is comparable to that of 1-hydroxypyrene that has a maximum peak at an excitation wavelength of 345 nm and an emission wavelength of 410 nm.

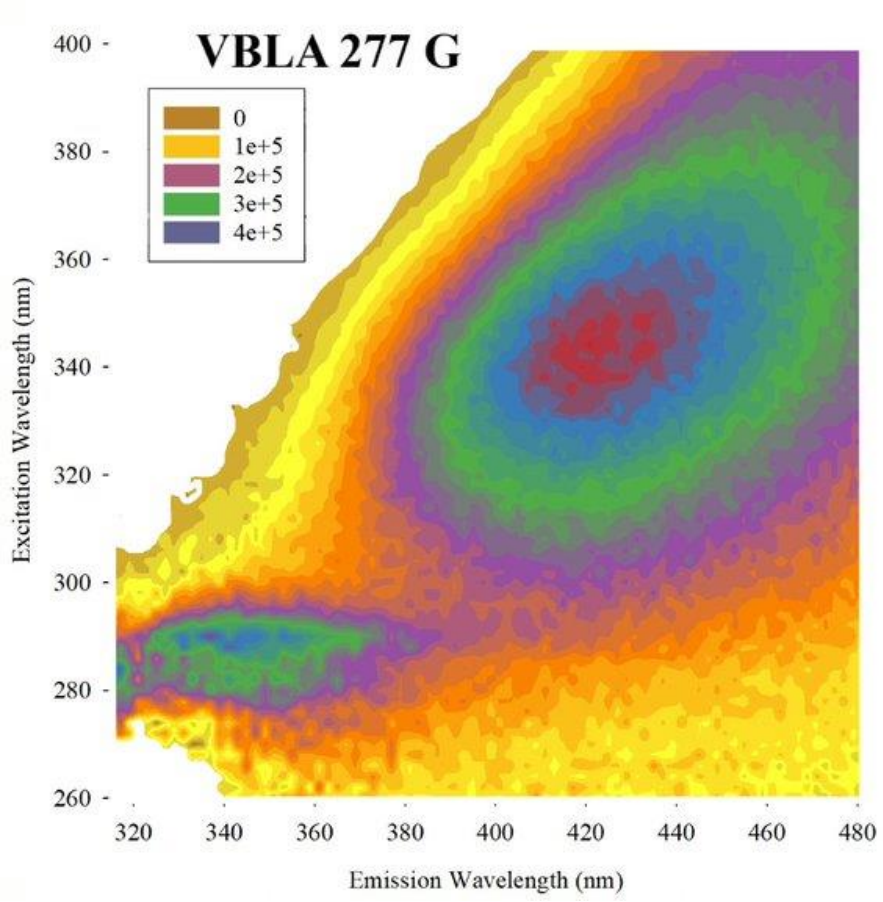

Figure 32: EEM spectrum of VBLA 277 gill extracted in 1 mL of 75% ethanol.

The EEM spectrum of VBLA 277 G can be seen in Figure 32. The excitation spectrum is observed between wavelengths 260-400 nm and the emission spectrum is observed between wavelengths 315-480 nm. Two maximal signals can be seen. The first at an excitation wavelength of 290 nm and an emission wavelength of 350 nm. This peak is comparable to that of crude oil that has a maximum peak at an excitation wavelength of 300 nm and an emission wavelength of 360 nm. The second maximal signal can be seen at an excitation wavelength of 350 nm and an emission wavelength of 420 nm. This peak is comparable to that of 1-hydroxypyrene that has a maximum peak at an excitation wavelength of 345 nm and an emission wavelength of 410 nm.

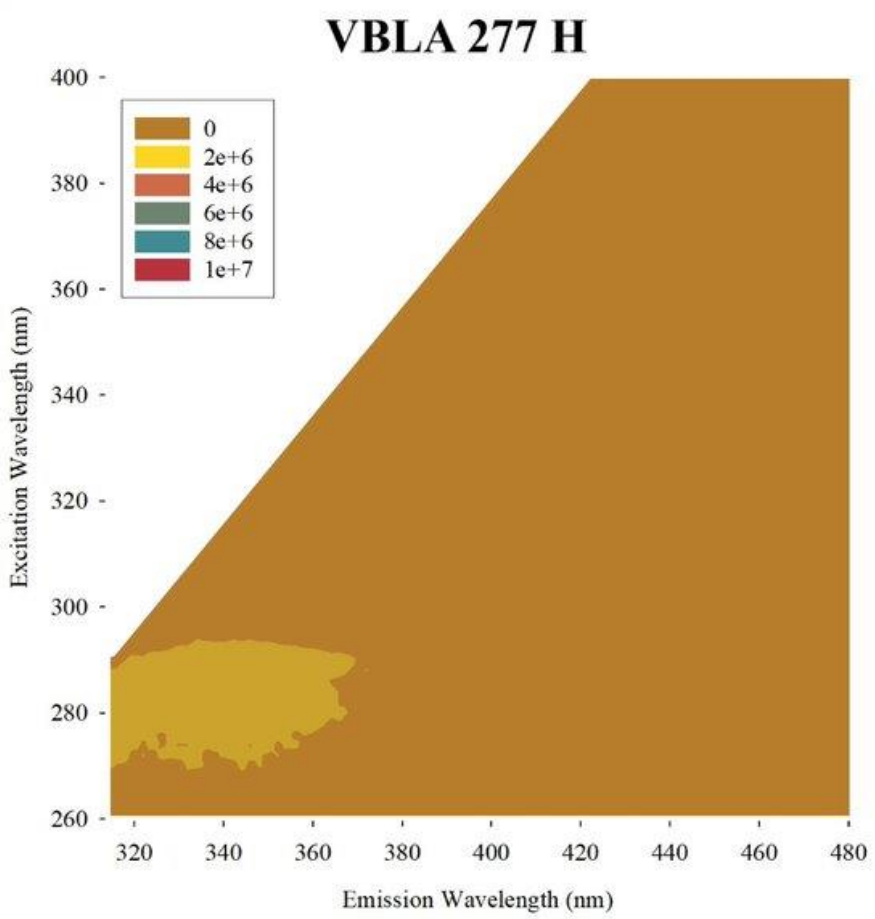

Figure 33: EEM spectrum of VBLA 277 heart extracted in 1 mL of 75% ethanol.

The EEM spectrum of VBLA 277 H can be seen in Figure 33. The excitation spectrum is observed between wavelengths 270-290 nm and the emission spectrum is observed between wavelengths 320-370 nm. One maximal signal can be seen at an excitation wavelength of 280 nm and an emission wavelength of 330 nm. This peak is comparable to that of albumin that has a maximum peak at an excitation wavelength of 280 nm and an emission wavelength of 330 nm.

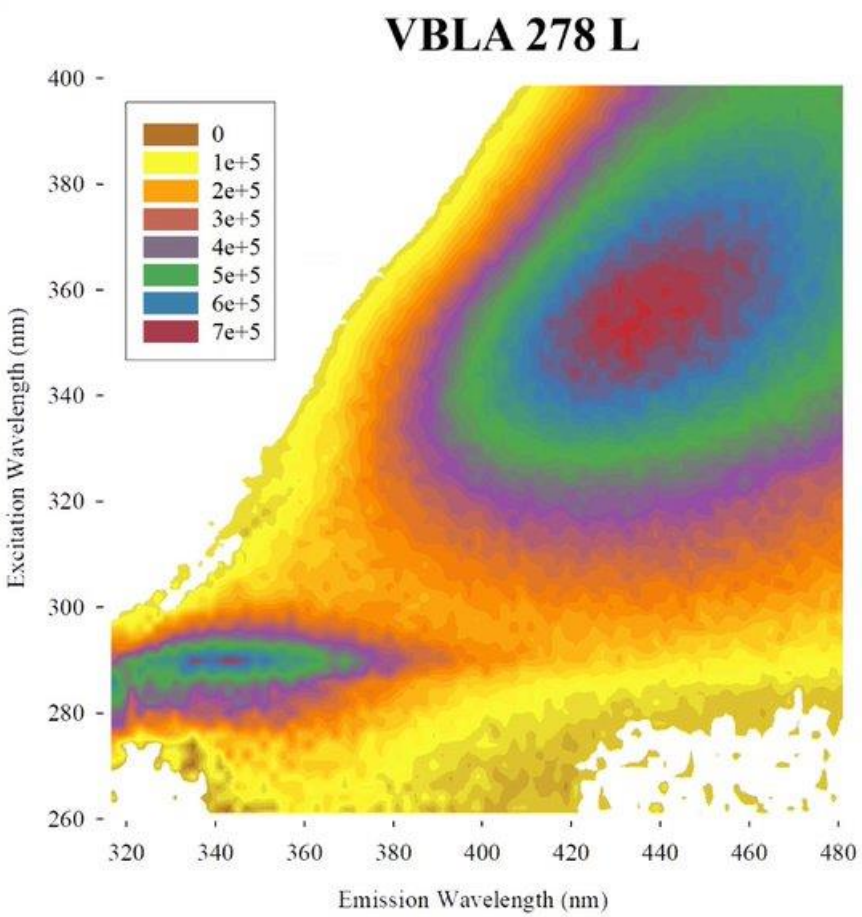

Figure 34: EEM spectrum of VBLA 278 liver extracted in 1 mL of 75% ethanol.

The EEM spectrum of VBLA 278 L can be seen in Figure 34. The excitation spectrum is observed between wavelengths 260-400 nm and the emission spectrum is observed between wavelengths 315-480 nm. Two maximal signals can be seen. The first at an excitation wavelength of 290 nm and an emission wavelength of 340 nm. This peak is comparable to that of crude oil that has a maximum peak at an excitation wavelength of 300 nm and an emission wavelength of 360 nm. The second maximal signal can be at an excitation wavelength of 340 nm and an emission wavelength of 440 nm. This peak is comparable to that of 1- hydroxypyrene that has a maximum peak at an excitation wavelength of 345 nm and an emission wavelength of 410 nm.

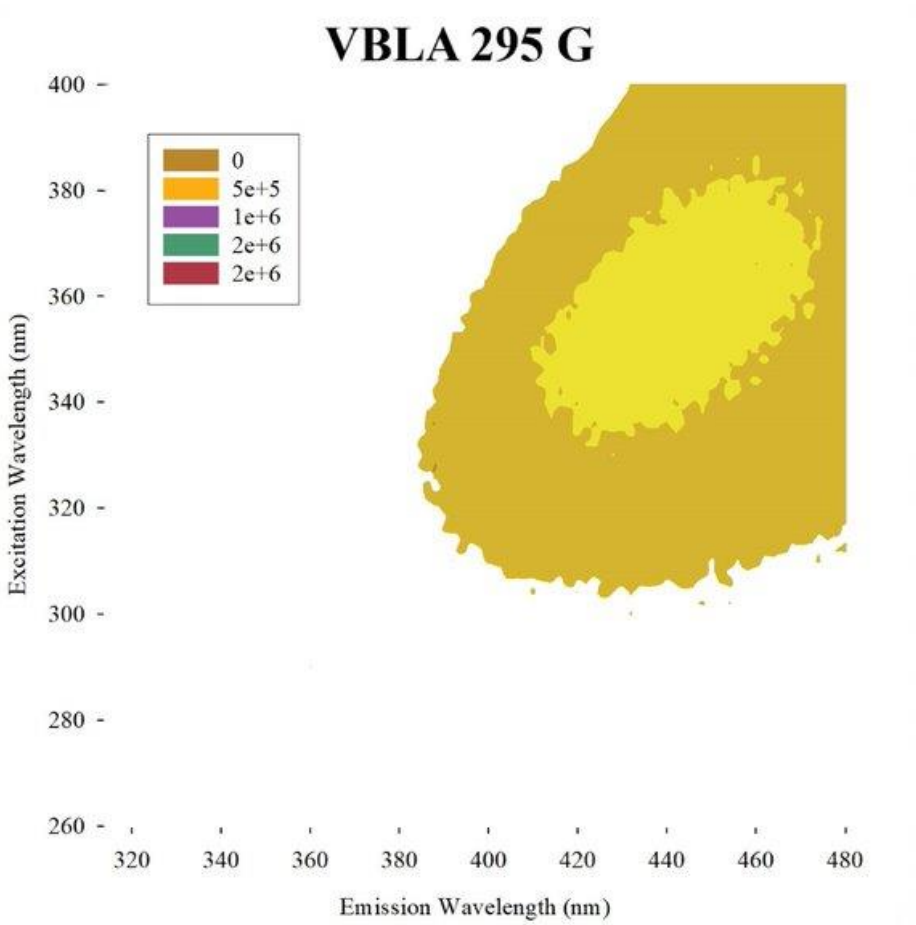

Figure 35: EEM spectrum of VBLA 295 gill extracted in 1 mL of 75% ethanol.

The EEM spectrum of VBLA 295 G can be seen in Figure 35. The excitation spectrum is observed between wavelengths 300-400 nm and the emission spectrum is observed between wavelengths 380-480 nm. One maximal signal can be seen at an excitation wavelength of 330 nm and an emission wavelength of 450 nm. This peak is comparable to that of that of benzo [a] pyrene that has a maximum peak at an excitation wavelength of 315 nm and an emission wavelength of 435 nm.

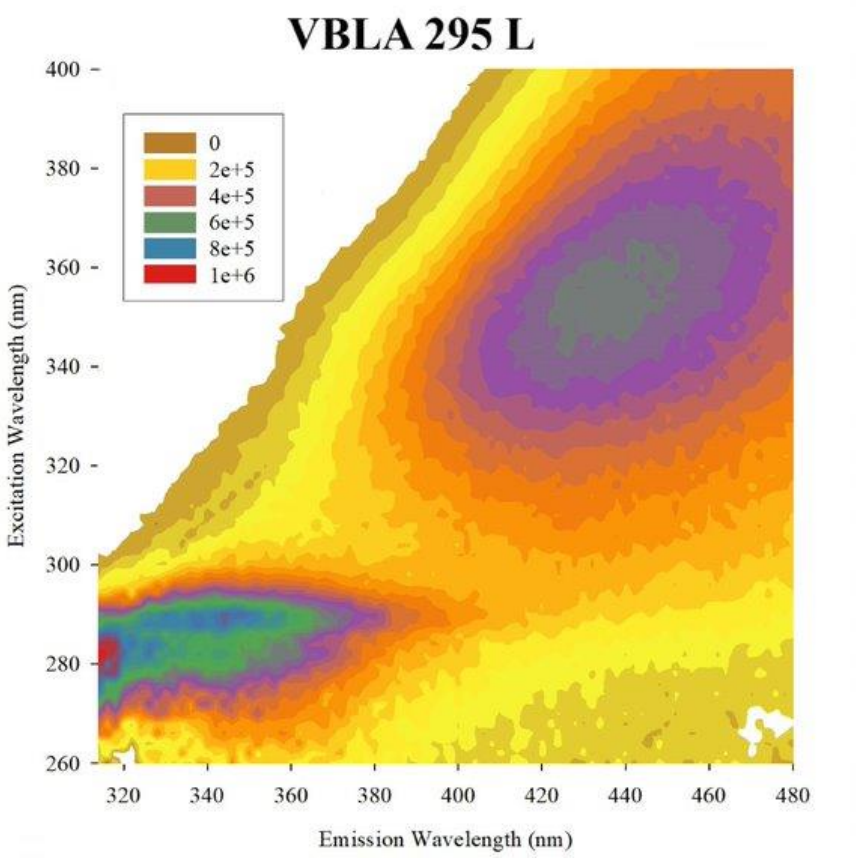

Figure 36: EEM spectrum of VBLA 295 liver extracted in 1 mL of 75% ethanol.

The EEM spectrum of VBLA 295 L can be seen in Figure 36. The excitation spectrum is observed between wavelengths 260-400 nm and the emission spectrum is observed between wavelengths 315-480 nm. Two maximal signals can be seen. The first at an excitation wavelength of 290 nm and an emission wavelength of 340 nm. This peak is comparable to that of crude oil that has a maximum peak at an excitation wavelength of 300 nm and an emission wavelength of 360 nm. The second maximal signal can be at an excitation wavelength of 340 nm and an emission wavelength of 440 nm. This peak is comparable to that of 1- hydroxypyrene that has a maximum peak at an excitation wavelength of 345 nm and an emission wavelength of 410 nm.

When comparing the crude oil spectra scan to that of the PAH standards, the hydroxylated PAH standards have emission and excitation maxima shifts to the red consistent with the addition of the -OH functionality (DeFelice, 2017). When compared to the raw crude oil, this shift in EEMs data in majority of organ extracts is strongly associated with the metabolites of the ingested PAHs. The naturally occurring proteins or vitamins tend to have EEMs behavior in the shorter wavelength spectral region. Further, previous work (Ridley) shows that the fluorescence quantum yield of majority of the biological fluorophores to possess quantum yields of 1×10^{-3} or less while the PAHs of interest have quantum yields of generally 0.1 or greater. As a result, high concentrations of biological fluorophores are required to stand out against the PAH signals. Almost all spectra (22) with exception of one sample (VBLA 277 H) confirmed exposure to PAH-like compounds in crude oil exposed fish. As seen in **Figures 17-23, 26, 27, 30 , 34** and **36.** the liver conveys the highest levels of fluorescence intensity when compared to the gill, gonad, heart, and muscle possibly due it being the major site of metabolism of hydrophobic contaminants. **Table 3** summarizes the fluorescence intensities conveying the liver to display the highest level of fluorescence intensity when compared to the other organs.

All GILA samples which directly received heavy oiling from the Deepwater Horizon (DWH) oil spill in 2010 crude oil-like fluorescence patterns conveying strong intensity signals. The majority of the scans displayed wavelength peaks consistent with the data for standard crude oil, albumin, 1-hydroxypyrene, and vitamin A. All VBLA samples which received less impact from the oil indicated crude oil-like fluorescence patterns conveying strong intensity signals with the exception of VBLA 277. When all spectra are compared to the raw crude oil, the fluorescence data is associated with long excitation wavelengths (i.e. red shifted) suggesting the metabolism of high molecular weight PAHs.

Fish	Heart (H)	Gill(G)	Muscle (M)	Liver(L)	Gonad(D)
VBLA 270				3.5×10^5	
VBLA 271	6×10^5	2.5×10^5		5×10^5	
VBLA 272				7×10^5	
VBLA 276	2×10^5	1.4×10^5	2×10^5	2×10^6	
VBLA 277	$1 \text{ x} \times 10^7$				2×10^5
VBLA 278				7×10^5	
VBLA 295		4×10^5		8×10^5	
GILA 420		2×10^5		2×10^5	3×10^5
GILA 520				4×10^5	
GILA 527				5×10^5	
GILA 531				7×10^5	
GILA 554				7×10^5	
GILA 560				7×10^5	

Table 3: Summary of fluorescence intensity in the long wavelength emission region.

Polymorphisms in the DNA binding domain of *p53* were evaluated using PCR followed by SSCP. Primers displayed in **Table 1** amplified a single band of 360 bp from genomic DNA of experimental fish. Various fish tissues were evaluated for polymorphisms following exposure of the 2010 Deepwater horizon oil spill. Since the liver is the major site of PAH metabolism into active metabolites that show genotoxicity, liver tissues were first analyzed followed by other organs to determine variability in organ polymorphism susceptibility in respect to PAH damage. Various organs (heart, gill, gonad, muscle, and liver) were homogenized and isolated using DNAzol showed inconsistency in quality or purity as seen in **Table 4.** Initial PCR reactions were

all set up using the DNA concentration yields that allowed for optimal template DNA concentrations.

Sample	Purity 260/280	Concentration (µg/µL)
GILA 420 D	1.70	0.085
GILA 420 G	1.72	0.090
GILA 420 L	1.80	0.035
GILA 520 L	1.79	0.045
GILA 521 G	1.71	0.089
GILA 521 M	1.40	0.032
GILA 521 H	1.80	0.049
GILA 524 L	1.83	0.359
GILA 524 H	1.87	0.153
GILA 527 L	1.79	0.045
GILA 531 L	1.69	0.035
GILA 534 M	1.40	0.031
GILA 534 L	1.71	0.067
GILA 554 L	1.80	0.039
GILA 560 D	1.80	0.022
GILA 560 M	1.34	0.027
GILA 560 G	1.31	0.046
GILA 560 L	1.77	0.006
GILA 560 H	1.79	0.017

VBLA 270 L	1.65	0.033
VBLA 271 H	1.74	0.037
VBLA 271 G	1.80	0.041
VBLA 271 L	1.72	0.035
VBLA 272 L	1.74	0.069
VBLA 276 G	1.81	0.071
VBLA 276 H	1.79	0.042
VBLA 276 L	1.75	0.071
VBLA 276 M	1.80	0.069
VBLA 277 G	1.69	0.034
VBLA 277 H	1.78	0.055
VBLA 279 D	1.70	0.071
VBLA 279 L	1.71	0.094
VBLA 279 M	1.59	0.051
VBLA 279 G	1.81	0.031

Table 4: Gulf menhaden spectrophotometry data

Table 4 displays experimental samples of all organs for DNA purity and concentration. Purity was calculated using the standard equation of purity= (A260/A280), where optimal double stranded DNA will have a purity of 1.8. Concentration was calculated from the equation dsDNA= 50µg/mL x O.D 260x dilution factor (Barbas, 2001).

The success of the DNA isolations was verified by amplifying two control samples (GILA 554L and VBLA 271 L) using primers specific to the *Fundulus heteroclitus* housekeeping gene beta-actin. Results demonstrate intense bands present at 150 bp for beta actin

in the control samples confirming successful DNA isolations (Note: this gel is not included in the figures of the results section). After this verification, various samples were chosen to test functionality of proposed primer set F4 and R0. **Figure 37** shows both GILA and VBLA liver samples were successfully amplified at 360 bp. These samples include VBLA 271 L, VBLA 276 L, VBLA 272 L, VBLA 279 L, GILA 526 L, GILA 560 L, GILA 527 L, and GILA 554 L. This primer set was selected for continued study**. Figure 38** shows data for other primer sets (F4R1 and F3R2) that were tested but did not demonstrate optimal results so they were discontinued.

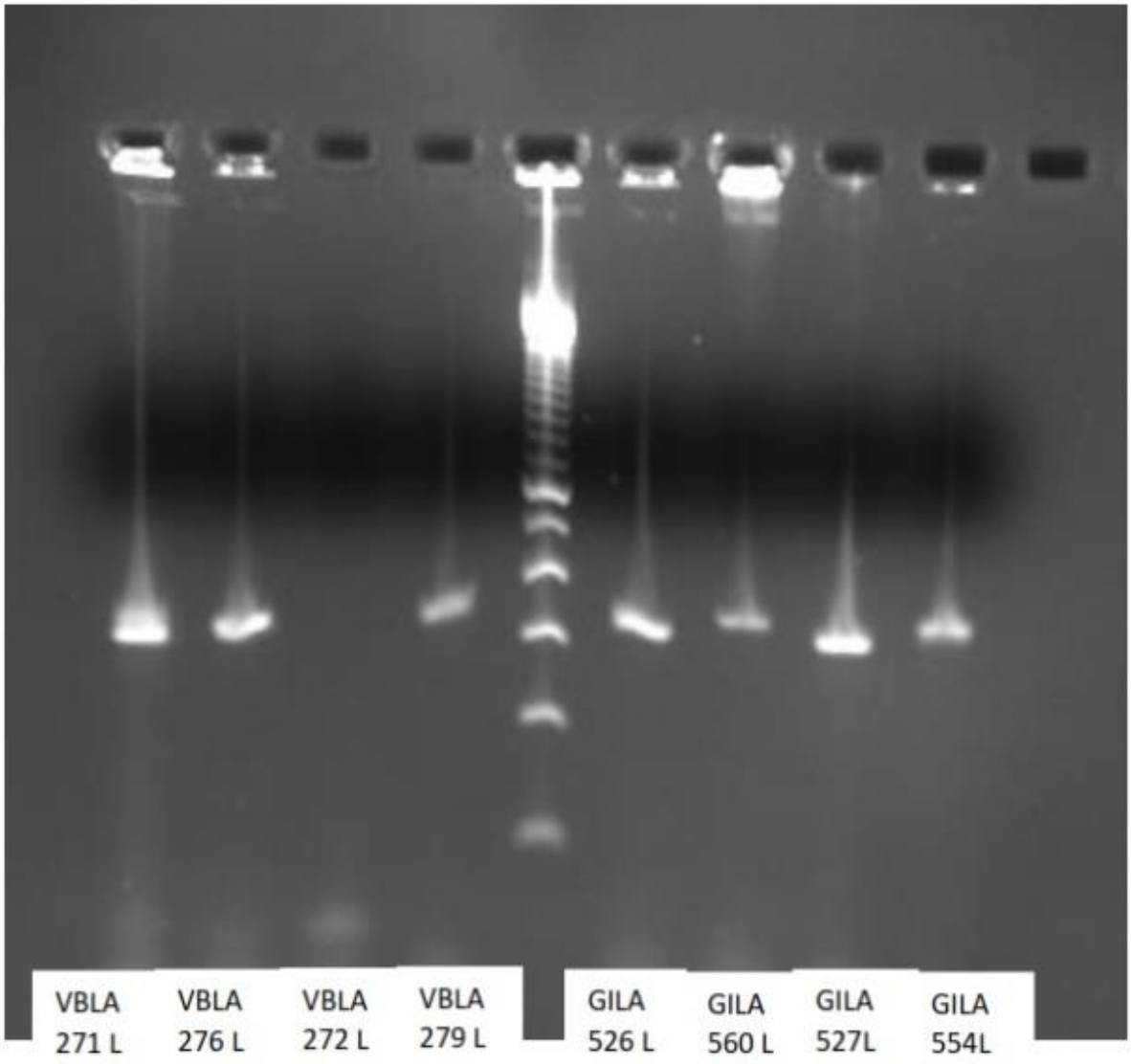

Figure 37: Verification of DNA integrity through F4 R0 primer set

Figure 37 shows an agarose gel testing the functionality of the proposed primers (F4 R0). A primer set was considered successful if it generated a sharp band approximately equal to the expected size of the *p53* DNA binding region template (360 bp). This gel utilizes a 100 DNA bp ladder. Bands at approximately 360 bp was indicative of successful amplification of this gene.

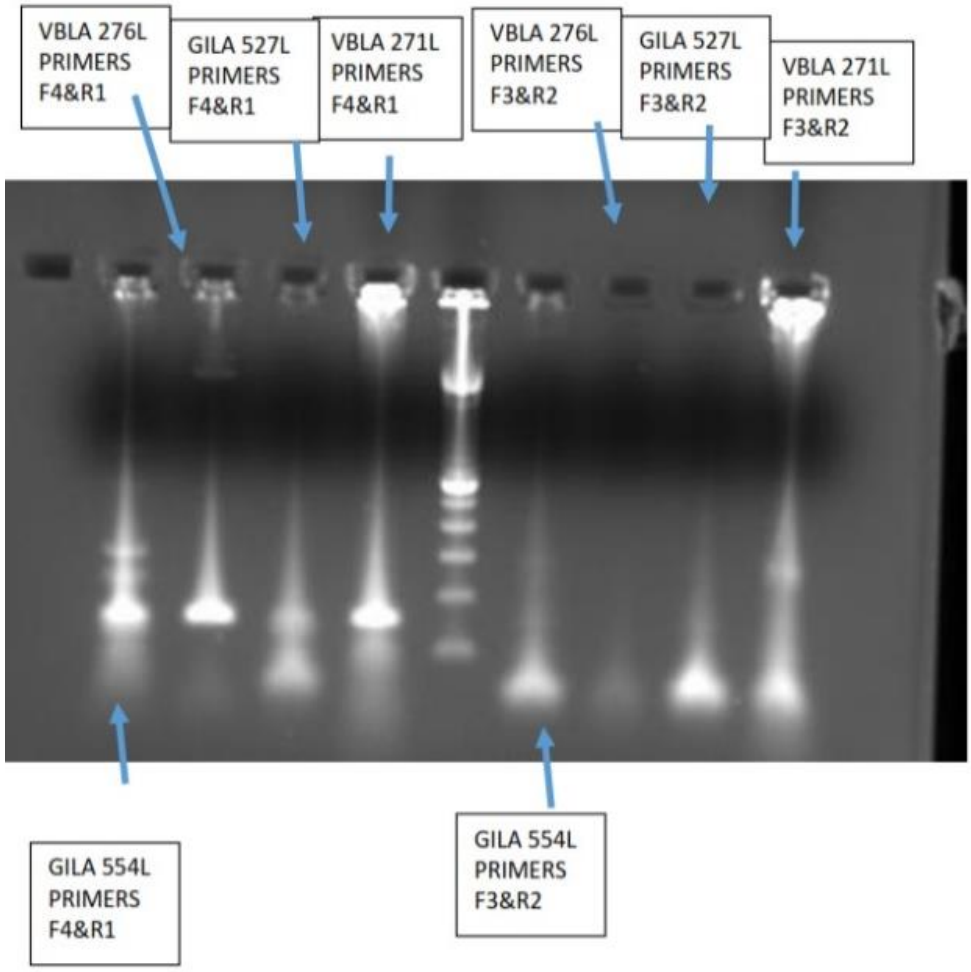

Figure 38: Evaluation of various primer sets to determine optimal binding

Figure 38 illustrates the two different primer sets (F4R1, F3R2) that were designed in attempt for amplification. Primer sets F4R1 and F3R2 combinations do not show successful amplification of the DNA binding domain.

Primer set F4 R0 illustrates successful amplification of the intended gene and was further continued in the study. All DNA samples underwent PCR, gel analysis, and then SSCP. **Figure 39** illustrates the successful PCR amplification from remaining samples. These samples include VBLA 270 M, VBLA 270 H, VBLA 591 G, VBLA 591H, VBLA 591 L, VBLA 591 M, VBLA 295 L, VBLA 295 G, VBLA 295 H, VBLA 279 M, VBLA 271 H, VBLA 271 G, VBLA 277 G, VBLA 277 H, VBLA 272 H, VBLA 272 M, VBLA 276 G, VBLA 276 H, and VBLA 276M. The

intended amplicon was 305 bp, however the actual amplicon was 360 bp indicating additional bases from an intron, later confirmed through sequencing.

Comparison of SSCP gels identified one profile in all organs of all subjects furthermore indicating low incidence of gene variation or singe nucleotide polymorphism (SNP). **Figure 40** demonstrates the consistent one profile shown at 100 bp and 300 bp in all samples. This shows high genetic relatedness among fish organs furthermore displaying no mutations and very little variation in the organs at the genetic level. This little variation was consistently seen in band intensity, relative size of the bands, and distance from one another.

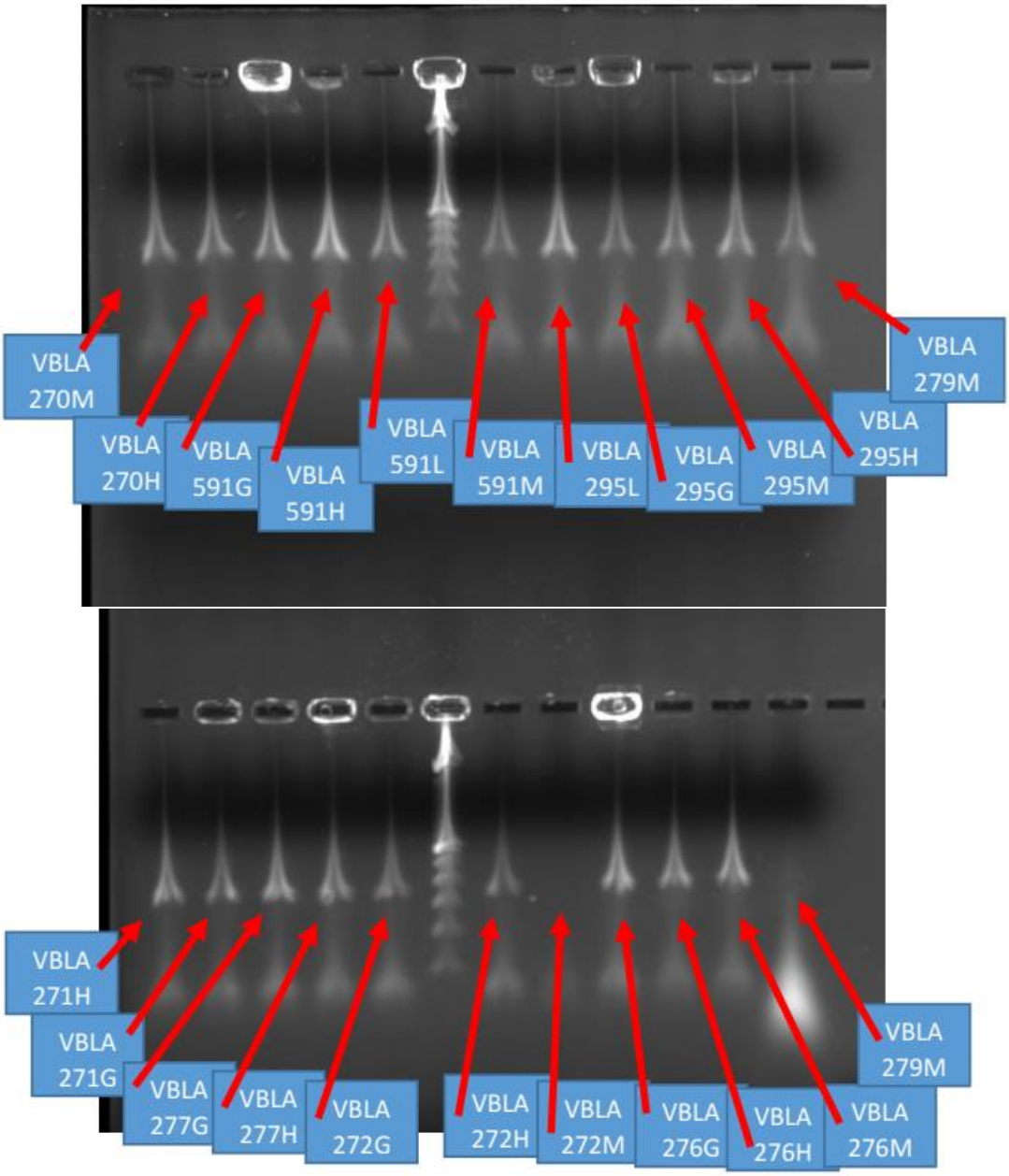

Figure 39: Evaluation in functionality of DNA integrity of different tissues with primer set F4 and R0

Figure 38 demonstrates a successful gel displaying consistent bands at approximately 360 bp which is equal to the expected size of the DNA binding region.

Figure 40: SSCP variant profiles of VBLA and GILA organ comparison

Figure 40 demonstrates single stranded conformational polymorphism profiles for both VBLA and GILA sample fish. SSCP profiles show a consistent band located at both 100 and 300bp.

Discussion

Oil spills have occurred more frequently since the oil industry began extracting oil from offshore sources and transporting it via large vessels. The 2010 Deepwater Horizon oil spill in the Gulf of Mexico is one of the most significant due to breakdown of an off-shore oil rig. The low molecular weight (LMW) PAHs (three aromatic rings or less) remain at the ocean surface and degrade with time due to natural weathering processes. They tend to cause an acute response. The high molecular weight (HMW) PAHs (four or more rings) tend to deposit into sediments which can retain toxicity for many years, resulting in a chronic exposure (Reid, 2017). Even though these compounds are hydrophobic, they and their oxidation products are soluble in seawater and can be easily taken up through skin contact, inhalation, and ingestion where they tend to concentrate in tissues such as liver, fat, and kidneys to further cause harm (Uversky, 2016). This study aimed to better understand the environmental impact of a high magnitude oil spill in an ecosystem through molecular techniques. The goal was to determine whether the DNA in certain organs in the exposed Gulf menhaden, *Brevoortia patronus*, were more susceptible to polymorphisms than others when exposed to PAH contamination. The use of fluorescent spectroscopy to verify PAH contamination, combined with PCR-SSCP techniques aimed to evaluate genotoxicity as shown by polymorphisms of the *p53* gene.

Mutations at the DNA binding domain of key regulatory genes such as *p53* can permanently block the normal functioning of the *p53* protein, that of inhibiting cell growth and division when excessive DNA damage is present. This dysfunction prevents cells containing defective genes from being removed by apoptosis, and allows them to further accumulate, ultimately forming tumor (Rust, 2004). *Brevoortia patronus*, or gulf menhaden, were chosen as the model toxicological organism due to their filter feeding lifestyle. They consume

phytoplankton and are an important link between producer and secondary consumer in the food-chain. The expectation of this study was that wild caught menhaden exposed to a catastrophic oil spill would serve to identify an organ more susceptible to polymorphisms with respect to PAH damage. This was accomplished by amplifying the DNA binding domain of the tumor suppressor gene *p53* to evaluate if oil exposure ultimately leads to polymorphisms in the genome.

The first step in evaluating the effects of PAHs is verification of the presence of these potent contaminants in these organs through excitation-emission matrix fluorescence spectroscopy. Excitation emission matrix scans were utilized as a technique to characterize the PAH presence through spectra affiliated with distinct patterns. These three-dimensional spectra are unique enough to be specifically correlated to known PAHs. Since the liver is the major site of PAH metabolism into active metabolites that show genotoxicity, liver tissues were first analyzed followed by other organs to determine variability in organ polymorphism susceptibility in respect to PAH damage. All samples had liver, gonad, muscle, gill, and heart extracted to determine the presence of PAHs and their metabolites. **Figure 4** illustrates standards composed of common PAHs. 3D scans of all standards indicate a specific pattern which is associated with individual variants of PAHs. All 3D scans from all organs indicated PAH profiles consistent with low and high molecular weight PAH parent compounds and metabolites in addition to biological fluorophores. The raw crude oil emission and excitation pattern is prevalent in a majority of fish organs in combination with a shift of HMW PAH metabolism. It's also important to note the quantum yields for the standards were 100x less when compared to the organs. Overall, the fluorescence spectroscopy verified the presence of these contaminants and their genotoxic metabolites. A summary of the fluorescence intensities in **Table 3** convey the liver to display the highest level of fluorescence intensity when compared to the other organs.

The effects of PAH metabolism during crude oil exposure is further explored through DNA isolation and analysis of the *p53* binding domain using PCR-SSCP. Through this technique, one can identify subtle differences in sequences (often a single base pair) which results in a different secondary structure and measurable difference in mobility through the gel. Literature strongly suggests a majority of mutations occur in the highly conserved region of the DNA binding domain of *p53* leading to the interest for this present study (Mason et al., 2012). The tumor suppressor gene *p53* plays a critical role in protecting the genome and cell cycle control by acting as a transcription factor binding to DNA response elements to elicit a cellular signal to activate a response (Johnsen et al., 2004). When mutated, uncontrolled cell growth is exhibited, which is a hallmark of various cancers. These mutations or polymorphisms can even be seen at the single base pair. **Figures 37** & **39** convey genomic analysis to show one consistent band at 360 bp in all fish samples which is consistent with the expected size of the DNA binding domain of *p53* displaying successful amplification of the gene.

Figure 40 shows the SSCP banding pattern of all experimental samples. This data establishes that the DNA polymorphisms were found in all organs of all fish samples. The samples demonstrated very similar profiles, which illustrates 2 bands; one at 300bp and the other at 100bp. This further indicates polymorphisms occurred less frequently that what was expected. One potential explanation is the bottleneck theory which postulates that a population can show a decrease in genetic diversity as a result of a catastrophic event (e. g. an oil spill). The theory indicates that an original population with high variability may experience a drastic reduction in population through a "bottleneck" or stressor to the environment which results in a new surviving population of reduced variability and higher genetic relatedness which was observed in the PCR-SSCP analysis (Saranjampour et al., 2017). This reduction in diversity can either select

for better adapted individuals but may also result in in-breeding with concomitant amplification of less productive genetic traits. In the case of the menhaden investigated, one can postulate that a decrease in the polymorphism of the p53 gene took place as the population experienced a severe decline in numbers. This suggests that further work into the decrease in p53 polymorphism induced by PAH contamination is a fertile field for further exploration.

References

Bentivegna, C. S., DeFelice, C. R., & Murphy, W. R. (2016). Excitation–emission matrix scan analysis of raw fish oil from coastal New Jersey menhaden collected before and after Hurricane Sandy. *Marine Pollution Bulletin*, *107*, 442–452.

Diercks, A.-R., Highsmith, R. C., Asper, V. L., Joung, D., Zhou, Z., Guo, L., Lohrenz, S. E. (2010). Characterization of subsurface polycyclic aromatic hydrocarbons at the Deepwater Horizon site. *Geophysical Research Letters; 37*(L2602) 6p.

Goto, D., & Wallace, W. G. (2011). Altered feeding habits and strategies of a benthic forage fish (Fundulus heteroclitus) in chronically polluted tidal salt marshes. *Marine Environmental Research*, *72*(1), 75–88.

Harvey, R. G. (1997). *Polycyclic aromatic hydrocarbons*. New York: Wiley.

Johnsen, A. R., & Karlson, U. (2004). Evaluation of bacterial strategies to promote the bioavailability of polycyclic aromatic hydrocarbons. *Applied Microbiology & Biotechnology*, *63*(4), 452–459.

Llamas, A., Al-Lal, A., García-Martínez, M., Ortega, M. F., Llamas, J. F., Lapuerta, M., & Canoira, L. (2017). Polycyclic Aromatic Hydrocarbons (PAHs) produced in the combustion of fatty acid alkyl esters from different feedstocks: Quantification, statistical analysis and mechanisms of formation. *Science of the Total Environment, 586*446-456. doi:10.1016/j.scitotenv.2017.01.180

Mason, O. U., Hazen, T. C., Borglin, S., Chain, P. S. G., Dubinsky, E. A., Fortney, J. L., Jansson, J. K. (2012). Metagenome, metatranscriptome and single-cell sequencing reveal microbial response to Deepwater Horizon oil spill. *ISME Journal: Multidisciplinary Journal of Microbial Ecology*, *6*(9), 1715–1727.

McCann, M.J., Able, K.W., Christian, R.R., Able, K.W., Fodrie, K.J,. Jensen, O.P., Johnson, J.J., Duarte, P.L., Martin, C.W., Olin, J.A., Polito, M.J., Roberts, B.J., Ziegler, S.L *(*2016). *Identifying key species in marsh food web responses to the Deepwater Horizon Oil Spill: a literature review. Coastal Waters Consortium II*

Millemann, D., Portier, R., Olson, G., Bentivegna, C., & Cooper, K. (2015). Particulate accumulations in the vital organs of wild *Brevoortia patronus* from the northern Gulf of Mexico after the Deepwater Horizon oil spill. *Ecotoxicology, 24*(9), 1831.

Mordukhovich, I., Pavel Jr., R., Terry, M.B., Santella, R., Zhang, Y.-J., Hibshoosh, H., Memeo, L., Mansukhani, M., Long, C.-M., Garbowski, G., Agrawal, M., Gaudet, M.M., Steck, S.E., Sagiv, S.K., Eng, S.M., Teitelbaum, S.L., Neugut, A.I., Conway-Dorsey, K., Gammon, M.D. (2010) Associations between polycyclic aromatic hydrocarbon-related exposures and p53 mutations in breast tumors. *Environmental Health Perspectives*, 118(4), 511-518.

Nadler, A. M., & Bentivegna, C. S. (2017). *Effects of Crude Oil on Tumor Suppressor P53 Polymorphisms in Laboratory-Exposed Killifish*. PowerPoint.

Nomura, T., Kamada, R., Ito, I., Sakamoto, K., Chuman, Y., Ishimori, K., Sakaguchi, K. (2011). Probing phenylalanine environments in oligomeric structures with pentafluorophenylalanine and cyclohexylalanine. *Biopolymers*, 95(6), 410–419.

Ozhan, K., Parsons, M. L., & Bargu, S. (2014). How Were Phytoplankton Affected by the Deepwater Horizon Oil Spill? *BioScience*, *64*(9), 829–836.

Reid, N. M., et al. (2017). The Landscape of Extreme Genomic Variation in the Highly Adaptable Atlantic Killifish. *Genome Biology and Evolution*, *9*(3), 659–676.

Retzlaff, M., Rohrberg, J., Küpper, N. J., Lagleder, S., Bepperling, A., Manzenrieder, F. Buchner, J. (2013). The Regulatory Domain Stabilizes the p53 Tetramer by Intersubunit

Contacts with the DNA Binding Domain. *Journal of Molecular Biology*, 425(1), 144–155. https://doi.org/10.1016/j.jmb.2012.10.015

Rust, A. J., Burgess, R. M., McElroy, A. E., Cantwell, M. G., & Brownawell, B. J. (2004). Influence of Soot Carbon on the Bioaccumulation of Sediment-Bound Polycyclic Aromatic Hydrocarbons by Marine Benthic Invertebrates: An Interspecies Comparison. *Environmental Toxicology & Chemistry*, *23*(11), 2594.

Saha, T., Kar, R. K., & Sa, G. (2015). Structural and sequential context of p53: A review of experimental and theoretical evidence. *Progress in Biophysics and Molecular Biology*, 117(2), 250–263.

Saranjampour, P., Vebrosky, E. N., & Armbrust, K. L. (2017). Salinity impacts on water solubility and n-octanol/water partition coefficients of selected pesticides and oil constituents. *Environmental Toxicology & Chemistry*, 36(9), 2274.

Schaefer, K. N., Geil, W. M., Sweredoski, M. J., Moradian, A., Hess, S., & Barton, J. K. (2015). Oxidation of p53 through DNA Charge Transport Involves a Network of Disulfides within the DNA-Binding Domain. *Biochemistry*, 54(3), 932–941.

Shukla, B., & Koshi, M. (2012). Importance of Fundamental sp, sp2, and sp3 Hydrocarbon Radicals in the Growth of Polycyclic Aromatic Hydrocarbons. *Analytical Chemistry*, *84*(11), 5007–5016.

Singleton, B., Turner, J., Walter, L., Lathan, N., Thorpe, D., Ogbevoen, P., & Reiss, K. (2016). Environmental stress in the Gulf of Mexico and its potential impact on public health. *Environmental Research, 146,*108-115.

Sunnucks, P., Wilson, A. C., Beheregaray, L. B., Zenger, K., French, J., & Taylor, A. C. (2000). SSCP is not so difficult: the application and utility of single-stranded conformation

polymorphism in evolutionary biology and molecular ecology. *Molecular Ecology*, 9(11), 1699–1710.

Uversky, V. N. (2016). p53 Proteoforms and Intrinsic Disorder: An Illustration of the Protein Structure-Function Continuum Concept. *International Journal of Molecular Sciences*, *17*(11), 1–37.